The Astrophysical Journal, 574:1039–1058, 2002 August 1

SPECTRAL PROPERTIES OF He AND HEAVY IONS IN ^{3}He-RICH SOLAR FLARES

G. M. Mason,[1,2] M. E. Wiedenbeck,[3] J. A. Miller,[4] J. E. Mazur,[5] E. R. Christian,[6] C. M. S. Cohen,[7] A. C. Cummings,[7] J. R. Dwyer,[8] R. E. Gold,[9] S. M. Krimigis,[9] R. A. Leske,[7] R. A. Mewaldt,[7] P. L. Slocum,[3] E. C. Stone,[7] and T. T. von Rosenvinge[6]

Received 2002 January 2; accepted 2002 April 8

ABSTRACT

Using advanced instrumentation on the *ACE* spacecraft, we have conducted a survey of solar energetic particle spectra in ^{3}He-rich events over a broad energy range ~80 keV nucleon^{-1} to 15 MeV nucleon^{-1} during the period 1997 September–2001 March. The spectra of ^{4}He and heavy ions (C, N, O, Ne, Mg, Si, S, Ca, Fe) were generally similar over this range but often hardened below ~1 MeV nucleon^{-1}. In most of the events there was even stronger hardening of the ^{3}He spectrum below ~1 MeV nucleon^{-1}, leading to an energy-dependent ^{3}He : ^{4}He ratio. These observations point to unique and distinct properties of ^{3}He in these events and place new constraints on models that seek to explain enhancements of ^{3}He and heavy ions using the same mechanisms. In addition to the events with spectra in the form of power laws or double power laws, there is a second class of event in which the low-energy ^{3}He and Fe spectra are rounded, while the ^{4}He remains a power law. In these cases ^{3}He and Fe spectra can be fitted at low energies by a stochastic acceleration model, but this model does not explain the higher energy portions of these spectra, nor the power-law spectral forms of the ^{4}He. These observations appear to require an additional mechanism, such as acceleration by cascading MHD turbulence. The ^{3}He enrichment pattern that we observe suggests that all these different spectral features might be due to processes with a common origin but then followed by different acceleration histories.

Subject headings: acceleration of particles — cosmic rays — interplanetary medium — solar wind — Sun: abundances — Sun: flares

1. INTRODUCTION

Solar energetic particle (SEP) events with enormous enhancements of ^{3}He have been observed for over 25 yr and have been the subject of many experimental and theoretical investigations since they gave promise of identifying a specific physical mechanism capable of causing the uniquely large enhancements (e.g., reviews by Kocharov & Kocharov 1984; Miller 1998; Reames 1999). Since it was well known that galactic cosmic rays are also enriched in ^{3}He as a result of spallation of ^{4}He in interstellar space, this possibility was initially considered for the ^{3}He-rich solar particle events but ruled out since other spallation products such as ^{2}H and ^{3}H were not observed (Garrard, Stone, & Vogt 1973). In addition to enhancements of ^{3}He : ^{4}He of up to ~10^4, ^{3}He-rich events show a number of features differing from large SEP events including enrichment of electrons relative to protons, enrichment of heavy-ion ratios (e.g., Ne/O, Fe/O) by factors of up to 5–20, and significantly higher heavy-ion ionization charge states (Luhn et al. 1985; Mason et al. 1986; Reames, Meyer, & von Rosenvinge 1994; Möbius et al. 1999). The events are also generally small in size and fail to exhibit association with coronal shocks or coronal mass ejections (CMEs) in contrast to the case for large solar particle events (Kahler et al. 1985). Taking account of these observational features, models for producing ^{3}He enrichments have generally included mechanisms that make use of the unique charge-to-mass ratio of ^{3}He (e.g., Fisk 1978; Varvoglis & Papadopoulos 1983; Temerin & Roth 1992; Miller, Viñas, & Reames 1993).

Although ^{3}He-rich events are often observed during solar active periods, and literally hundreds have been surveyed in the literature, the studies have been hampered because the low intensities make it difficult to accurately study the spectra or composition over a broad enough energy range to distinguish varying shapes or compositional features. Energy-dependent features including flattening of spectra below ~1 MeV nucleon^{-1} have been observed by several instruments, but statistical uncertainties and concern about possible contamination from other sources have made progress difficult (Möbius et al. 1980, 1982; Mazur, Mason, & Klecker 1995; Reames et al. 1997a).

These observational limitations were systematically addressed in the design of the *Advanced Composition Explorer* (*ACE*) mission, by including instruments with extremely large collecting power combined with excellent isotopic resolution. *ACE* instruments are able to resolve significant enhancements of ^{3}He in large shock-accelerated solar particle events and in association with interplanetary shocks as they pass by the spacecraft (Cohen et al. 1999; Mason, Mazur, & Dwyer 1999b; Wiedenbeck et al. 2000; Desai et al. 2001). In this work, however, we focus on the small, impulsive ^{3}He-rich particle events, in order to determine spectral and abundance features over a very broad energy range. In a prior report emphasizing events observed

[1] Department of Physics, University of Maryland, College Park, MD 20742; glenn.mason@umail.umd.edu.
[2] Institute for Physical Science and Technology, University of Maryland, College Park, MD 20742.
[3] Jet Propulsion Laboratory, California Institute of Technology, Pasadena, CA 91109.
[4] University of Alabama, Huntsville, AL 35899.
[5] Aerospace Corporation, El Segundo, CA 90245-4691.
[6] NASA Goddard Space Flight Center, Greenbelt, MD 20771.
[7] California Institute of Technology, Pasadena, CA 91125.
[8] Florida Institute of Technology, Melbourne, FL 32901.
[9] Johns Hopkins University/Applied Physics Laboratory, Laurel, MD 20723.

primarily at low energies, we described two classes of ^{3}He-rich events: class 1 had power-law or double power-law spectra that were similar for ^{3}He and other heavy ions; class 2 had curved ^{3}He and Fe spectra distinctly different from other species such as ^{4}He and O (Mason, Dwyer, & Mazur 2000). In the present work, we emphasize impulsive ^{3}He-rich events that produced significant ^{3}He intensities above $\sim$5 MeV nucleon^{-1}, in order to gain a broader picture of spectra and composition.

2. OBSERVATIONS

2.1. *Instrumentation*

The observations reported here were made with instruments on board the *ACE* spacecraft, which was launched into an orbit around the sunward Lagrangian point in 1997 August (Stone et al. 1998b). For measurements below a few MeV nucleon^{-1}, we used the Ultra Low Energy Isotope Spectrometer (ULEIS), a time-of-flight mass spectrometer with geometry factor of $\sim$1 cm^2 sr, and a 50 cm flight path (Mason et al. 1998). Above a few MeV nucleon^{-1}, we used observations from the Solar Isotope Spectrometer (SIS), a multidetector dE/dx versus residual energy spectrometer with two telescopes and a geometry factor of $\sim$38 cm^2 sr (Stone et al. 1998a). Each of these spectrometers measures particle trajectory within the telescope in order to achieve a combination of sensitivity and mass resolution far exceeding most previous instruments.

Figure 1 shows examples of He isotope peaks observed in small events such as those considered in this study. Panels (*a*) and (*c*) show peaks for ^{3}He : ^{4}He ratios of $\sim$10%, which was a typical selection threshold for previous studies. Panels (*b*) and (*d*) are examples of extremely large ^{3}He enrichments. For panels (*a*) and (*c*) showing smaller enhancements, note that the ^{3}He is easily resolved, with a ratio of the ^{3}He peak to the valley between ^{3}He and ^{4}He of greater than 10 : 1; this means that ratios down to 1% can be easily measured if counting statistics are sufficient. Even lower ratios can be measured by reducing background events using multiple time-of-flight or dE/dx measurements (Cohen et al. 1999; Mason et al. 1999b).

2.2. *Event Selection*

Since the purpose of this work is to examine ^{3}He-rich event spectra and composition in order to gain insights into the acceleration mechanism, it is important that the exam-

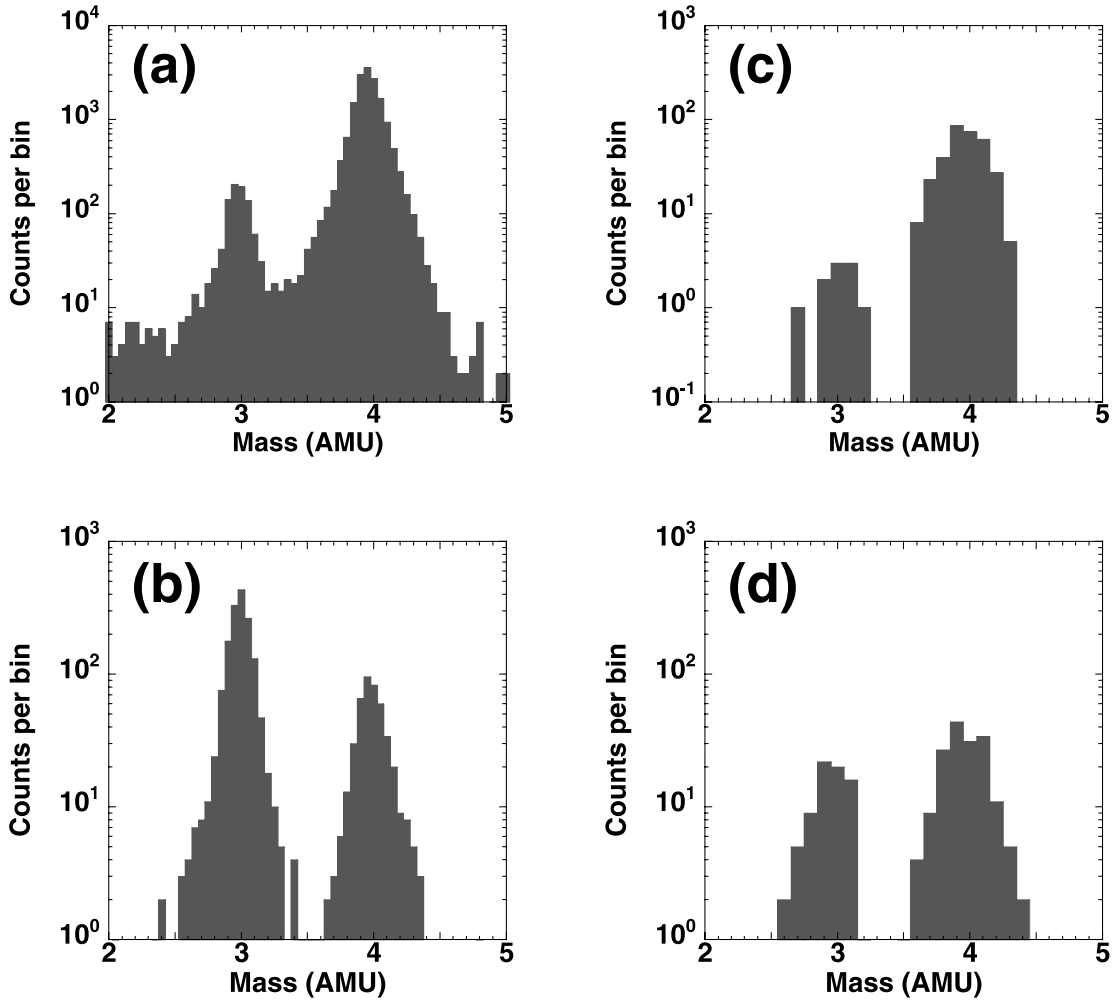

FIG. 1.—Sample ULEIS and SIS mass resolution showing examples of events with both large and small ^{3}He : ^{4}He ratios. ULEIS mass resolution for 0.75 MeV nucleon^{-1} for (*a*) the 1999 May 28 event and (*b*) the 1999 March 21 event. Sample SIS mass resolution near 7.5 MeV nucleon^{-1} for (*c*) 2000 January 18 and (*d*) 2000 September 27. Where available, multiple dE/dx measurements have been used to reduce background in the SIS histograms.

ples selected for study be samples of a single acceleration event at the Sun and therefore free of contamination from other particle sources. One such source is multiple ^{3}He events coming from the same active region, where velocity dispersion in the event is such that at a given time low-energy particles from a single event may be present at 1 AU along with higher energy particles from a later event at the Sun (Reames et al. 1997b; Mazur et al. 2000). To avoid this problem, we selected different time periods as a function of particle energy, thus separating multiple events (see discussion in Mason et al. 2000). The other main particle background source is from other events such as prior large solar particle events, corotating interaction regions, or interplanetary shocks. At low energies especially, these can produce intensity enhancements for days and will contaminate small ^{3}He-rich event spectra during that time. The contamination does not affect all species or energies equally: because of the relative abundances in the ^{3}He-rich events, ^{4}He is the most susceptible element for contamination, O and Fe are less susceptible, and ^{3}He is the least susceptible. Lower energy portions of spectra are usually more susceptible to contamination, but because of the hardening of corotating interaction region spectra late in the event (Mason et al. 1997; Reames et al. 1997b), contamination may also be important around $\sim$1 MeV nucleon^{-1} and less so at lower energies.

Event selection began with a survey of the SIS 1 hr average data ^{3}He intensity levels above 5.2 MeV nucleon^{-1} over the period 1997 September 1–2001 March 1. There were 37 periods found with significant increases, ranging in length from 14 to 72 hr. Roughly half of these periods showed sharp rises in ^{3}He intensity (time to maximum less than 3–4 hr), while the rest showed slower rises (time to maximum greater than 6 hr). Not all event onsets could be cleanly categorized as a result of low intensity levels. Many of the events with slower rises appeared to be due to multiple injections, but we kept only those where a single injection dominated. The remaining time periods were then examined at low energies (near 200 keV nucleon^{-1}). We selected only those cases in which there was a clear low-energy injection of ^{3}He or Fe and low interference from other particle sources. This left 14 events, which are listed in Table 1. Three of these events (4, 8, and 12) were in our earlier study of 12 ^{3}He-rich events emphasizing low energies (Mason et al. 2000).

Column (2) of Table 1 lists the onset day, and column (3) shows the start time obtained from the particle velocity dispersion extrapolated back to the Sun assuming a 1.2 AU interplanetary field line length and no scattering. Columns (4)–(9) list possible flare associations including flare importance, flare times, and associated active regions at the Sun (taken from the NOAA/Space Environment Center daily notices). Notice also that two of the eight identified events have likely origins in the eastern hemisphere, even though it is generally believed that since these events originate from compact regions on the Sun they must generally originate in the western hemisphere if they are to be observed at Earth. This may be due to uncertainties in the identification of the associated flare, which is common in these events since they are small (Kahler et al. 1985). It is also possible that connection to an impulsive event in the eastern hemisphere was obtained through connection inside a magnetic cloud (e.g., Larson et al. 1997; Reames et al. 1997a; Richardson et al. 2000).

Column (10) of Table 1 lists the particle event spectral class (see below), and columns (11)–(13) list the ^{3}He : ^{4}He ratio at low and high energy and the Fe/O ratio at low energy. Column (14) lists the type of rise observed at SIS as fast (<3–4 hr), slow (>5 hr), or multiple (probably several events occurred but are not clearly resolved). Eight of these events had fast rises at SIS energies, three were slow, and three were multiple. There is residual contamination of ^{4}He in some of these time periods, but detailed inspection indicates that in the worst case a few ^{4}He data points may have $\sim$50% contamination; for cases in which contamination was larger than this, or in cases at high energies where no significant intensity increase was observed, those points were deleted from the spectra.

Figure 2 shows an example of fast He intensity onsets from the event of 2000 May 1. The left panel shows intensities at three representative energies, and the right panel shows an all-ion spectrogram where the arrival time of each ion is plotted versus 1/(energy nucleon^{-1}). On the spectrogram, particles arriving along a field line of nominal 1.2 AU length will fall on a line parallel to the sloped lines starting at each day tick. Notice the very sharp rise starting around 12:00 UT on day 122, with particle arrivals at lower energies continuing later and later until around 24:00 when magnetic connection to the site is lost (see discussion in Mazur et al. 2000). There is then a connection to a filled flux tube just after the start of day 123, perhaps from the same event. After this, intensities drop significantly. In analyzing an event such as this one, we computed fluences using different time intervals at different energies, selecting only those particles from the single injection. This removes background particles from other sources as well as the intensity increase from the magnetic tube connection near the start of day 123. A more detailed discussion of this technique has been presented by Mason et al. (2000). The left panel of Figure 2 shows the intensity levels. Notice that at 5.2 MeV nucleon^{-1} the intensities jump almost 4 orders of magnitude in less than 1 hr; at 546 keV nucleon^{-1} the rise is also very sharp, while at 73 keV nucleon^{-1} the event is barely visible, so for this event the ion spectra were not reported below 100 keV nucleon^{-1}. While such fast, nearly scatter-free rises have been observed many times before with ^{3}He-rich events (e.g., Reames, von Rosenvinge, & Lin 1985; Mason et al. 1989), this event is unusually free of other backgrounds and was also associated with a narrow CME (Kahler, Reames, & Sheeley 2001).

Contrast the sharp rise seen in Figure 2 with the slow rise shown in Figure 3 for the 2000 September 27 event. Here the high-energy intensities take 7 or 8 hr to reach maximum, and much longer at lower energies. This is typical of the timing in so-called gradual solar particle events, and it can be seen that the event shows clear velocity dispersion expected from a single injection at the Sun. The ^{3}He : ^{4}He ratio in this event in fact exceeds that of the scatter-free event of Figure 2 at all energies (see Table 1). Many prior studies of ^{3}He-rich events have emphasized their nearly scatter-free propagation (e.g., Zwickl et al. 1978; Möbius et al. 1980; Reames et al. 1985; Mason et al. 1989). This created something of a puzzle since the event acceleration is believed to be at the Sun, and the scatter-free behavior depends on the state of the interplanetary medium, so there is no identified physical link between the two properties. Figure 3 shows that, indeed, ^{3}He-rich events can have gradual time-intensity profiles. This was probably missed in the earlier work as a result of the combination of lower sensitivity and resolution of the instruments as compared with ULEIS and SIS.

TABLE 1

^{3}He-rich Solar Flare Time Periods

Number (1)	Start Day (2)	Start Time (DOY) (3)	IMP[a] (4)	Optical Flare Start Time (5)	Location (6)	X-Ray Flare (1–8 Å) (7)	X-Ray Flare Start (UT) (8)	Active Region (9)	Class[b] (10)	^{3}He/^{4}He (385 keV neutron^{-1}) (11)	^{3}He/^{4}He (6.72 MeV neutron^{-1}) (12)	Fe/O (385 keV neutron^{-1}) (13)	Rise at Greater than 5 MeV neutron^{-1}[c] (14)
1.....	1997 Nov 29	332.58	...	...	...	M1.1	1954	...	1	0.100 ± 0.023	0.715 ± 0.071	...	F
2.....	1998 May 28	148.50	...	...	N20W80	Many C	...	8226?	1*	0.043 ± 0.002	0.170 ± 0.014	0.36 ± 0.01	M
3.....	1998 Aug 13	225.5	SF	1754	S25W61	C9.5	1750	8293	1	0.151 ± 0.010	0.784 ± 0.043	1.21 ± 0.19	F
4.....	1998 Sep 9	252.17	...	...	S22W60	M2.8	0452	8323?	1*	0.211 ± 0.007	0.201 ± 0.017	1.76 ± 0.11	F
5.....	1999 Mar 21	80.17	...	...	...	...	...	...	2	1.672 ± 0.074	0.739 ± 0.096	2.22 ± 0.28	M
6.....	1999 Mar 22	81.83	...	...	...	...	...	...	1	1.246 ± 0.151	6.570 ± 0.593	2.18 ± 0.96	F
7.....	1999 Jun 18	169.33	SF	1444	N26W53	C2.2	1433	8582	1	0.115 ± 0.004	0.351 ± 0.016	1.20 ± 0.09	S
8.....	1999 Aug 7	219.76	SF	1727	N18W40	M1.2	1852	8656	2	0.809 ± 0.060	2.580 ± 0.220	1.49 ± 0.22	F
9.....	1999 Oct 22	295.75	SF	1405	N20W76	C3.4	1404	8732	1	0.056 ± 0.017	0.125 ± 0.023	0.44 ± 0.20	M
10.....	1999 Nov 1	305.00	SF	0133	S19E15	C3.7	0130	8749	1	0.170 ± 0.038	1.110 ± 0.103	1.15 ± 0.70	F
11.....	2000 Jan 18	18.50	SF	0949	S14W38	M1.2	0936	8824	1*	0.088 ± 0.003	0.124 ± 0.008	0.55 ± 0.05	F
12.....	2000 May 1	122.42	...	...	N20W54	M1.1	1016	8976[d]	1*	0.062 ± 0.006	0.057 ± 0.008	2.22 ± 0.15	F
13.....	2000 Sep 27	271.17	1N	0307	N18W56	C9.6	0305	9167	1	0.080 ± 0.003	0.859 ± 0.028	0.66 ± 0.04	S
14.....	2000 Dec 28	363.00	SF	2211	S14E16	C5.8	2209	9283	1	0.156 ± 0.014	0.476 ± 0.027	1.62 ± 0.17	S

[a] Flare importance; optical, X-ray, and active region identification from NOAA/Space Environment Center.

[b] ^{3}He-rich flare spectral classification (see text); an asterisk denotes events that have similar spectra for ^{3}He and ^{4}He below $\sim$1 MeV nucleon^{-1}.

[c] F: fast; S: slow; M: likely multiple injections.

[d] See discussion in Kahler et al. 2001.

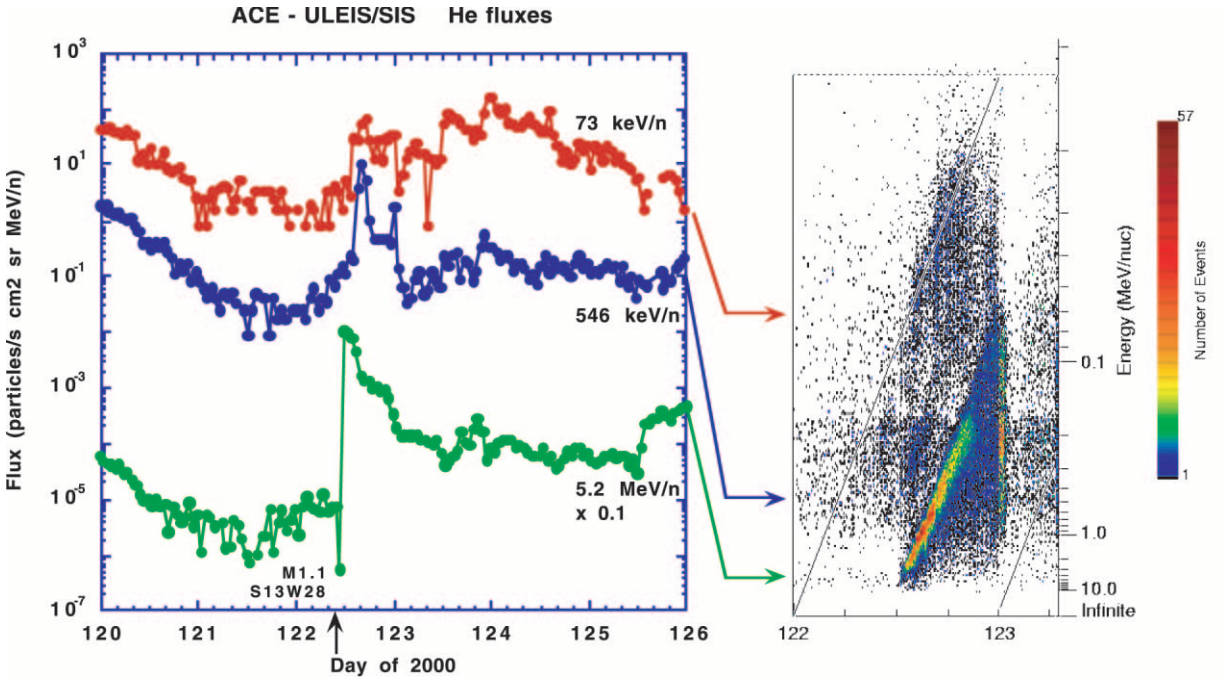

FIG. 2.—*Left panel:* 1 hr average He count rate intensities for the fast rise event of 2000 day 122 (May 1) at three representative energies. *Right panel:* Spectrogram of all ions plotted as 1/ion speed vs. time of arrival. Arrows indicate energy of the count rate intensities on the spectrogram.

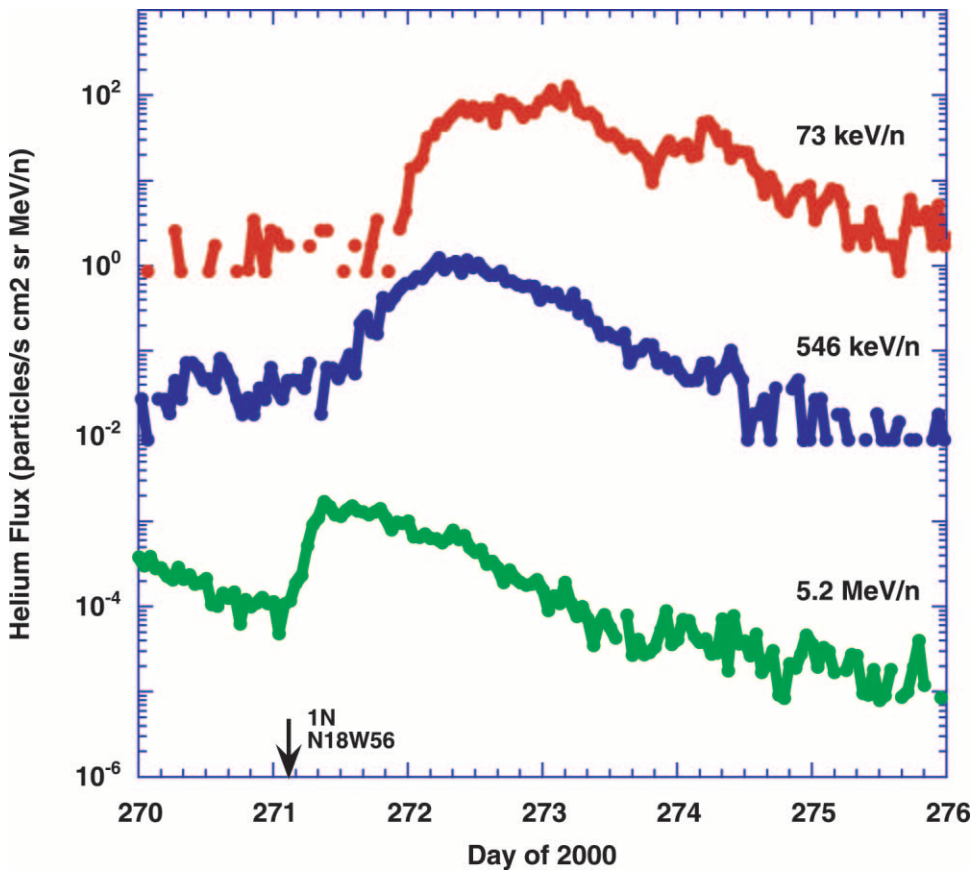

FIG. 3.—1 hr average He count rate intensities for the slow rising event of 2000 day 271 (September 27) at three representative energies

2.3. *Spectra for Individual Events*

We now examine examples of spectral forms of several events. Figure 4 shows fluence spectra ^{3}He, ^{4}He, ^{16}O, and Fe for the 1998 September 9 event (number 4 in Table 1). This event is one of the two events in the survey that produced significant numbers of ions heavier than He in the SIS energy range (the other is 2000 May 1). The spectral forms for all the elements are quite similar in this event. Below $\sim$1.5 MeV nucleon^{-1} the spectra can be fitted with a power law in kinetic energy $dJ/dE \propto E^{-\gamma}$, with γ in the range 1.15–1.38. About $\sim$2 MeV nucleon^{-1} the spectra steepen significantly with $\gamma = 3.4$–3.9. In order to compare the shapes of other heavy-element spectra in this event, Figure 5 shows the ratios of major heavy-ion species compared to oxygen. The figure shows that within uncertainties the ratios are basically constant in energy, except for ^{3}He, which increases by $\sim$50% compared to O over the range from 150 keV nucleon^{-1} to 1.5 MeV nucleon^{-1} (see further discussion below). Following our earlier study emphasizing low energies, this spectral type is called "class 1" as a result of the presence of power-law spectra (Mason et al. 2000).

Figure 6 shows another example of a class 1 event wherein the ^{4}He, O, and Fe are power laws with only a modest rollover toward higher energies, but the ^{3}He spectrum is much harder than the other ions below 1–2 MeV nucleon^{-1}. The ^{3}He : ^{4}He ratio in this event increases from $\sim 0.028 \pm 0.002$ at 135 keV nucleon^{-1} to 0.94 ± 0.02 at 5.2 MeV nucleon^{-1}. In contrast to the strong variation of the ^{3}He : ^{4}He at lower energies, above $\sim$5 MeV nucleon^{-1} this ratio stays relatively constant for a range of several MeV nucleon^{-1}. The question arises whether at the highest energies in the figure the ^{4}He could be dominated by, e.g., anomalous cosmic-ray ^{4}He, causing the observed drop in the ^{3}He : ^{4}He ratio. That is not the case: even at the highest energies, the ^{4}He hourly intensities showed a significant increase in this event such that the vast majority of the counts making the highest energy point are from the solar particle event.

Figure 7*a* shows the second general type of spectral form we encountered, wherein the ^{4}He is a double power law while the ^{3}He and Fe spectra curve over toward lower energies. The O spectrum shows a low-energy turnover like Fe, but the more limited energy range makes it difficult to distinguish whether it is curved or a double power law. Notice in particular that the ^{3}He : ^{4}He ratio varies from $\sim$0.4 to 3.6, almost an order of magnitude. Again, following our earlier study, we classify these spectral types as "class 2." Table 1 lists the classifications for each of the events: of the 14 events, 12 are class 1 and two are class 2. There are several additional features to note in Figure 7*a*: based on the lower energy data one might expect that the ^{3}He : ^{4}He ratio would continue to fall above $\sim$3 MeV nucleon^{-1} or that the spectra might continue to drop as an exponential in energy per nucleon. Neither is observed: the ^{3}He : ^{4}He ratio does continue to drop, but not a great deal, and the spectra harden into power laws in energy over the range $\sim$5–10 MeV nucleon^{-1}. The rollovers of the ^{3}He and Fe spectra occur at distinctly different energies, suggesting that a kinetic energy per nucleon spectral form may not be the proper representation of these spectra. Figure 7*b* explores this question by

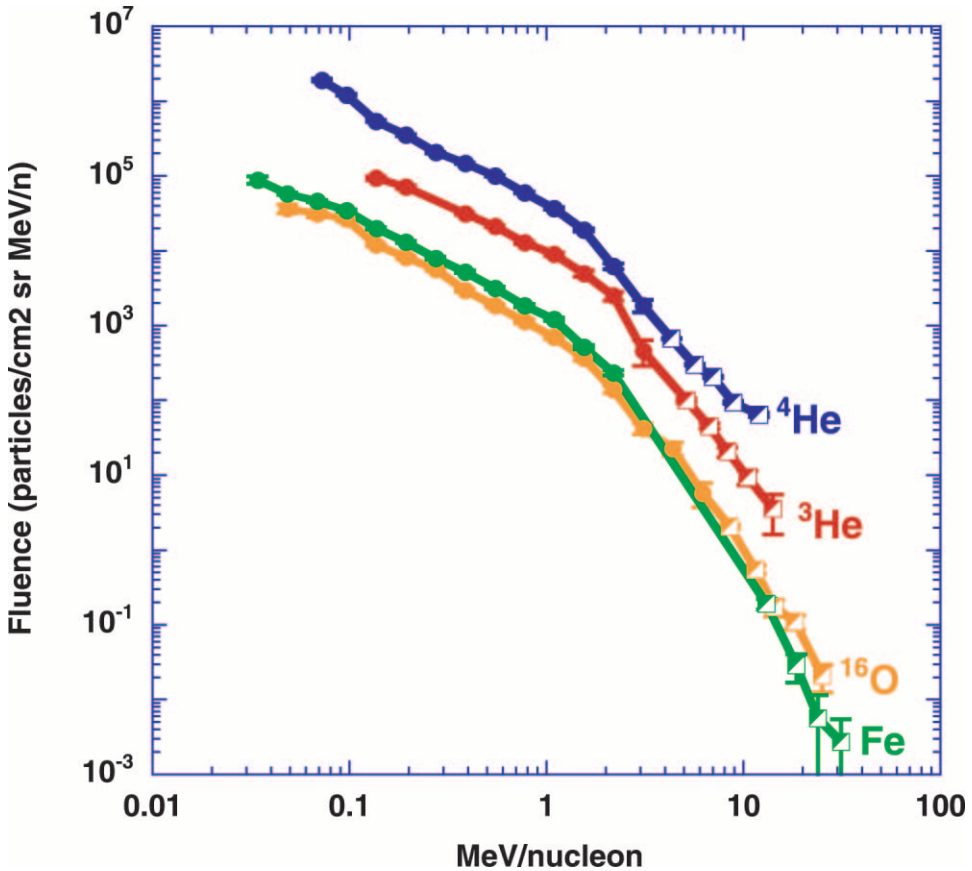

FIG. 4.—Fluences for the 1998 September 9 event, plotted vs. kinetic energy per nucleon. *Filled circles:* ULEIS measurements; *half-filled squares:* SIS measurements.

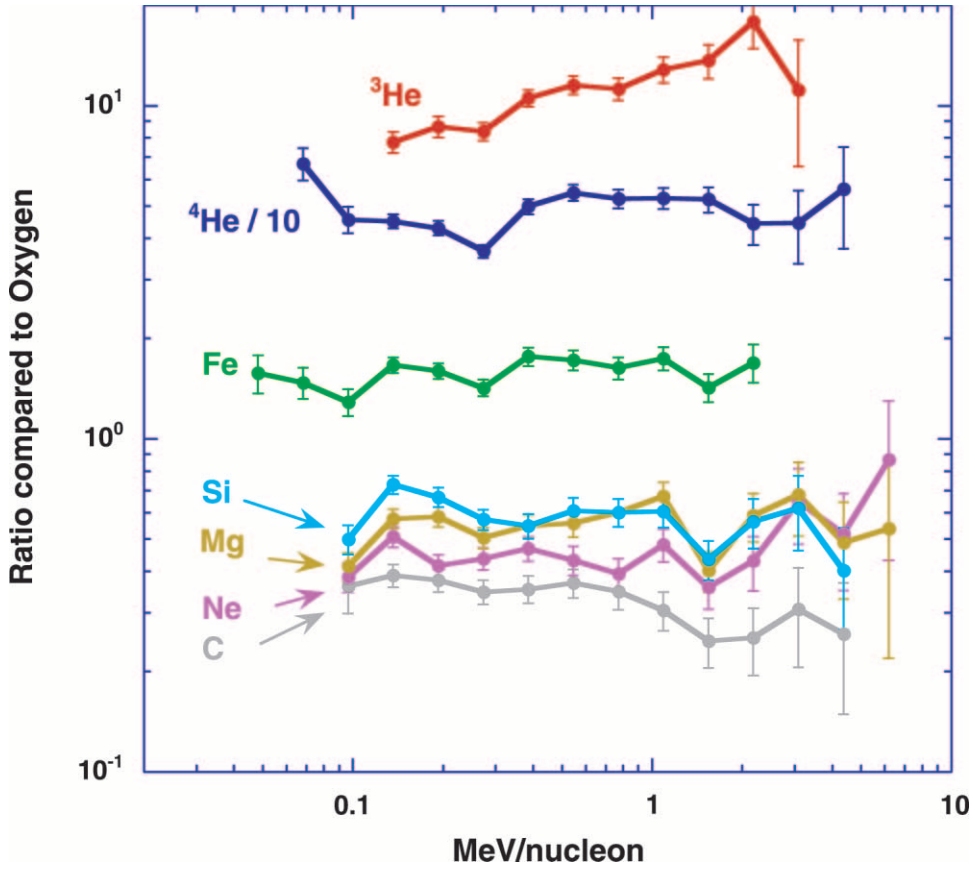

FIG. 5.—Ratios of major heavy elements to oxygen for the 1998 September 9 event

plotting the same points as functions of magnetic rigidity (momentum per unit charge) assuming that the ionization states are typical of impulsive solar particles observed in other events with *ACE* instruments (i.e., fully stripped except for Fe, which has $Q \sim 19$; Möbius et al. 2000). Since the ^{3}He charge-to-mass ratio is much higher than for Fe, the rollover features seen in Figure 7*a* will lie closer to each other when plotted versus magnetic rigidity, as shown in Figure 7*b*. However, although the spectral forms are more similar as functions of rigidity, still an additional factor of 2 adjustment [e.g., spectra depending on $(A/Q)^2$] would be required to align the Fe and ^{3}He spectra. Even if such a selection of independent variable could be justified, we would still be left with a very large variation of the ^{3}He : ^{4}He ratio in this event.

Figure 8 shows the ^{3}He : ^{4}He ratios for the three examples discussed here. Notice that for the class 1 event on 1998 day 252 the ratio is generally consistent with a single value, with some drop-off at energies approaching 10 MeV nucleon^{-1}. The second class 1 event (2000 day 271) shows a factor of $\sim$30 rise in ^{3}He : ^{4}He, peaking at $\sim$5 MeV nucleon^{-1} before dropping off again by a factor of 2 toward higher energies. The class 2 event of 1999 day 80 has a peak in the ^{3}He : ^{4}He ratio at about 1 MeV nucleon^{-1}, with drop-offs of a factor of 10 toward both higher and lower energies.

2.4. *Spectral Properties*

We now examine spectral features for the whole group of 14 events. In doing this we use the ^{4}He spectrum as the basis for comparison since it is measured with greatest accuracy and over the largest energy range of the elements available in this study. Because of the general similarity of the ^{4}He spectrum with those of other heavy ions, the properties seen when comparing to ^{4}He should generally apply to oxygen, Fe, etc., although curvature observed in the Fe spectrum may be an exception in some cases.

Examining the ^{4}He spectra in Figures 4, 6, and 7*a*, it is evident that power-law spectra are reasonable fits over limited portions of the energy range, with a break occurring around 1–2 MeV nucleon^{-1}. We therefore characterize the spectra in terms of the spectral index γ with assumed spectra form $dJ/dE \propto E^{-\gamma}$, where J is the fluence and E is energy per nucleon. Values of γ were fitted using a least-squares technique over the energy ranges 0.1–1.0 and 1.0–10.0 MeV nucleon^{-1}. In a couple of cases, the location of the "break" in the spectral form and/or particle counting statistics required that these energy intervals be adjusted slightly (<20%) to fit the data.

A comparison between the spectral indices of O and ^{4}He is shown in Figure 9*a*, with filled circles showing the range $\sim$0.1–1 MeV nucleon^{-1} and open circles showing $\sim$1–10 MeV nucleon^{-1}. The points are spread around the diagonal line, confirming the impression from the individual cases examined above that the O and ^{4}He spectra are similar over this entire energy range. The steepening of the spectra between low and higher energies is also clearly seen from the higher spectral index values for the 1–10 MeV nucleon^{-1} data. For the low-energy range, where spectral indices from all 14 events are available, the average difference between the γ-values of O and ^{4}He is 0.06 ± 0.26. In the high-energy range, where nine spectra could be measured, the difference

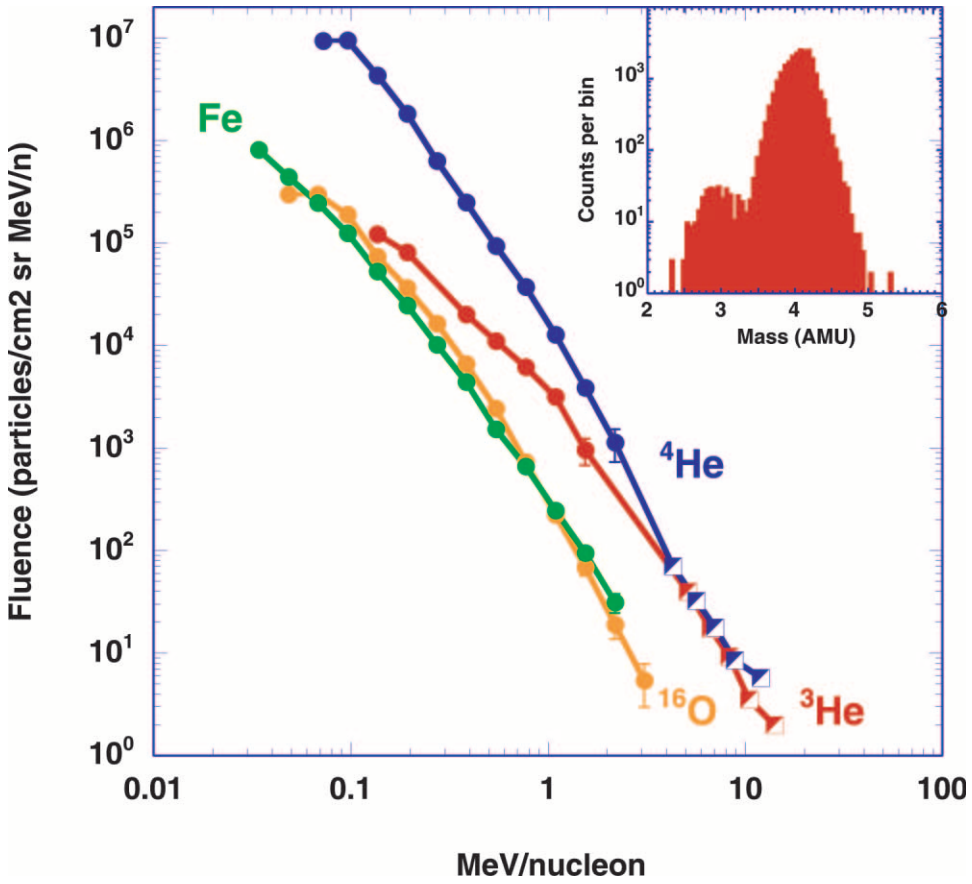

FIG. 6.—Fluences for the 2000 September 27 event, plotted vs. kinetic energy per nucleon. *Symbols:* Same as Fig. 4. *Inset:* Mass histogram for ^{3}He and ^{4}He region for 160–220 keV nucleon^{-1}.

is 0.08 ± 0.44. Based on the similarity of the ^{4}He spectrum to the O spectrum and the similarity of heavy-nuclei spectra to the O spectrum as shown in Figure 5, we suggest that the ^{4}He spectra are similar to the heavy-ion spectra in all the class 1 events.

In order to examine the steepening of power-law spectra with more accuracy than possible using O, Figure 9*b* shows a plot of the ^{4}He spectral index at 1–10 MeV nucleon^{-1} versus the ^{4}He spectral index at 0.1–1.0 MeV nucleon^{-1}. Points falling on the diagonal line have the same spectral index, i.e., no break in the spectral form. One of the 14 events did not have a fitable spectrum at high energies and so is not shown. For the remaining 13, only one event (number 9, 1999 October 22) fell close to the diagonal line; all the rest had low-energy spectra significantly harder than above 1 MeV nucleon^{-1}. It can be seen from the figure that the 12 events that show a spectral break are fairly uniformly displaced from the diagonal, indicating that the *difference* in slopes between the higher and lower energy spectra falls in a rather narrow range. For these points, the average difference between the high- and low-energy γ-values is 1.28 ± 0.24.

Figure 9*c* compares the low-energy ^{3}He and ^{4}He spectral indices for the 12 class 1 events. All but one of the ^{3}He points lie to the right of the diagonal; i.e., the ^{3}He spectra are usually harder than the ^{4}He. Figure 9*c* also shows that many of the events have ^{3}He spectral indices close to 1: 10 of the 12 events have slopes that lie in the rather narrow range 0.86–1.28. It is evident from the figure that in fact the low-energy spectral indices from ^{3}He and ^{4}He are not well correlated; indeed, the regression coefficient between the two sets of points in Figure 9*c* is 0.34. For 12 points, there is about a greater than 20% chance of exceeding this correlation coefficient from a random population.

Figure 10 shows all the class 1 ^{3}He spectra (except numbers 1 and 10, which have large errors) after renormalizing to a common value at 1.1 MeV nucleon^{-1}. Events 2 and 13 have relatively steep spectral slopes below 1 MeV nucleon^{-1}, but the remaining eight events have spectral indices clustered around 1.0 below 1 MeV nucleon^{-1} and steepening to about 2 above that.

The relation between the ^{3}He and ^{4}He spectra at high (>1 MeV nucleon^{-1}) energies is quite different as shown for the class 1 events in Figure 11. In this energy range the ^{3}He spectral indices steepen and are scattered around the diagonal line. Although there is considerable scatter in the points, the systematic difference seen at low energies is absent.

The ^{3}He : ^{4}He ratio appears to be related to the spectral features we observe. The highest ^{3}He : ^{4}He ratios are in the class 2 events (see also Mason et al. 2000), although the extreme energy dependence of the ratio in these cases can result in energy regions where the ratio is not as large. Interestingly, for class 1 events the *high-energy* ^{3}He : ^{4}He ratio correlates with the *low-energy* spectral behavior of ^{3}He and ^{4}He. Thus, for the high-energy data the eight events with ^{3}He spectra distinctly harder than ^{4}He have an average ^{3}He : ^{4}He ratio of 1.80 ± 3.08 (the large dispersion is due to event 6), while the four events with ^{3}He spectra similar to

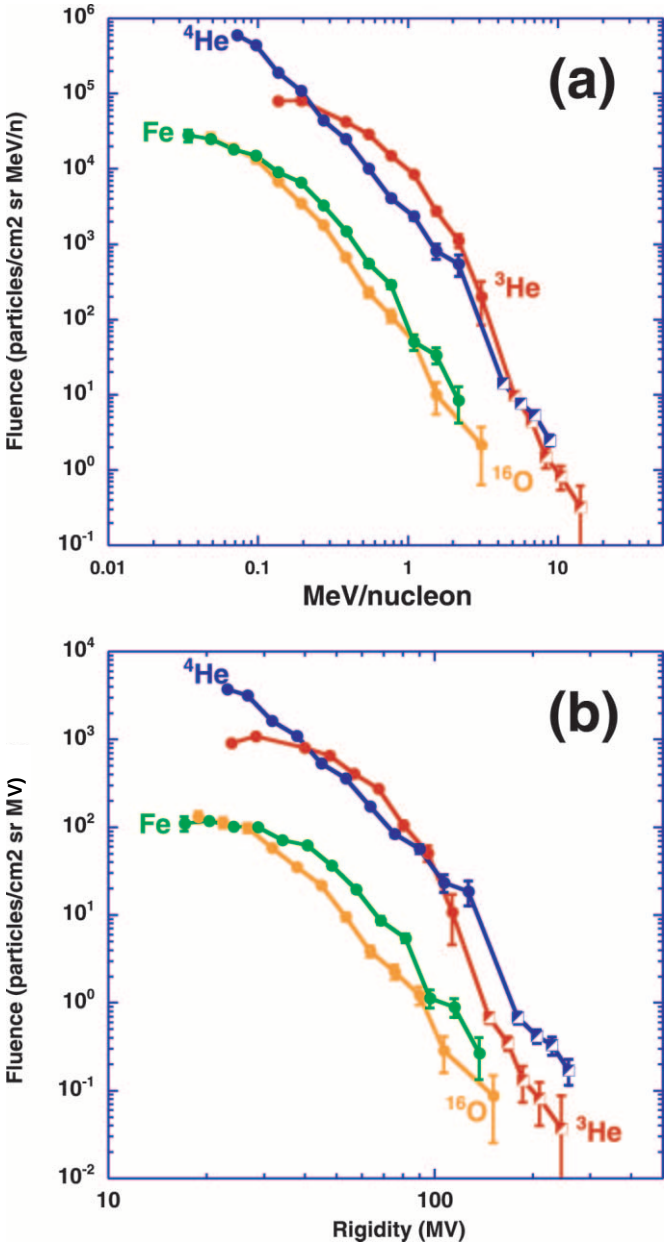

FIG. 7.—Fluences for the 1999 March 21 event. *Symbols:* Same as Fig. 4. (*a*) Fluence vs. MeV nucleon^{-1}; (*b*) Fluence vs. rigidity.

^{4}He have a significantly lower average ^{3}He : ^{4}He ratio of 0.14 ± 0.08, as shown in Figure 12 (the dividing line chosen was $\gamma^3\mathrm{He}/\gamma^4\mathrm{He} \sim 0.8$).

2.5. *Composition*

Table 2 lists the average abundances of heavy ions for this survey, along with atomic parameters including first ionization potential (FIP). The composition was measured over the energy interval 250–500 keV nucleon^{-1}, with the values calculated as an unweighted average of the relative abundances in each of the 14 events in Table 1. Figure 13 compares these low-energy composition values with the impulsive event composition at higher energy from a survey at ~2.5 MeV nucleon^{-1} (Reames 1999). The similarity between the two sets of data is striking considering the large difference in energy and the fact that the surveys used completely different sets of events. This broadens the evidence that the heavy-ion abundances of ^{3}He-rich SEP events show a characteristic pattern, as first pointed out by Mason et al. (1986) for a survey near 1.5 MeV nucleon^{-1}. The sixth column of Table 2 has a comparison of ^{3}He-rich SEP abundances in this survey with average abundances in a survey of over 50 large, gradual SEP events (Reames 1999). Compared to the large SEP events, elements in the range Ne–S are enhanced by a factor of 2–3, and Fe is enhanced by a factor of ~10. The observed enhancement pattern is plotted as a function of both mass and FIP in Figure 14. Since the gradual SEP abundances used as a reference already contain an enhancement of low-FIP elements (Reames 1999), the pattern shown in the figure is in addition to this baseline FIP bias. Considering the uncertainties in the data, the enhancements are reasonably well ordered by mass (and therefore also by atomic number and charge-to-mass ratio). Plotting the data versus FIP does not produce as clear an ordering in the data: for example, Mg and Fe have FIP values differing by only ~0.2 eV, and yet Fe is consistently enhanced much more than Mg in these events. Similarly, Mg and Ne show similar enhancements even though their FIP values differ by about 14 eV. Thus, the well-known enhancements of SEPs and slow solar wind by FIP when compared to photospheric abundances (Breneman & Stone 1985; von Steiger & Geiss 1989; Reames 1995; von Steiger, Geiss, & Gloeckler 1997) do not order the enrichment pattern observed in ^{3}He-rich events compared to slow solar

TABLE 2

^{3}He-RICH SOLAR FLARE ABUNDANCES

Element	Mass	Atomic Number	FIP	Abundance (375 keV nucleon^{-1})	Relative to Gradual SEPs[a]
He	4	2	24.46	57.15 ± 7.79	1.00 ± 0.15
C	12	6	11.22	0.35 ± 0.08	0.75 ± 0.16
N	14	7	14.48	0.22 ± 0.06	1.79 ± 0.46
O	16	8	13.55	$\equiv 1.00 \pm 0.14$	$\equiv 1.00 \pm 0.15$
Ne	20	10	21.47	0.34 ± 0.06	2.22 ± 0.39
Mg	24	12	7.61	0.41 ± 0.07	2.07 ± 0.36
Si	28	14	8.12	0.43 ± 0.06	2.83 ± 0.41
S	32	16	10.30	0.19 ± 0.04	5.89 ± 1.16
Ca	40	20	6.09	0.21 ± 0.09	19.53 ± 8.22
Fe	56	26	7.83	1.21 ± 0.14	9.04 ± 1.08

[a] Reames 1999.

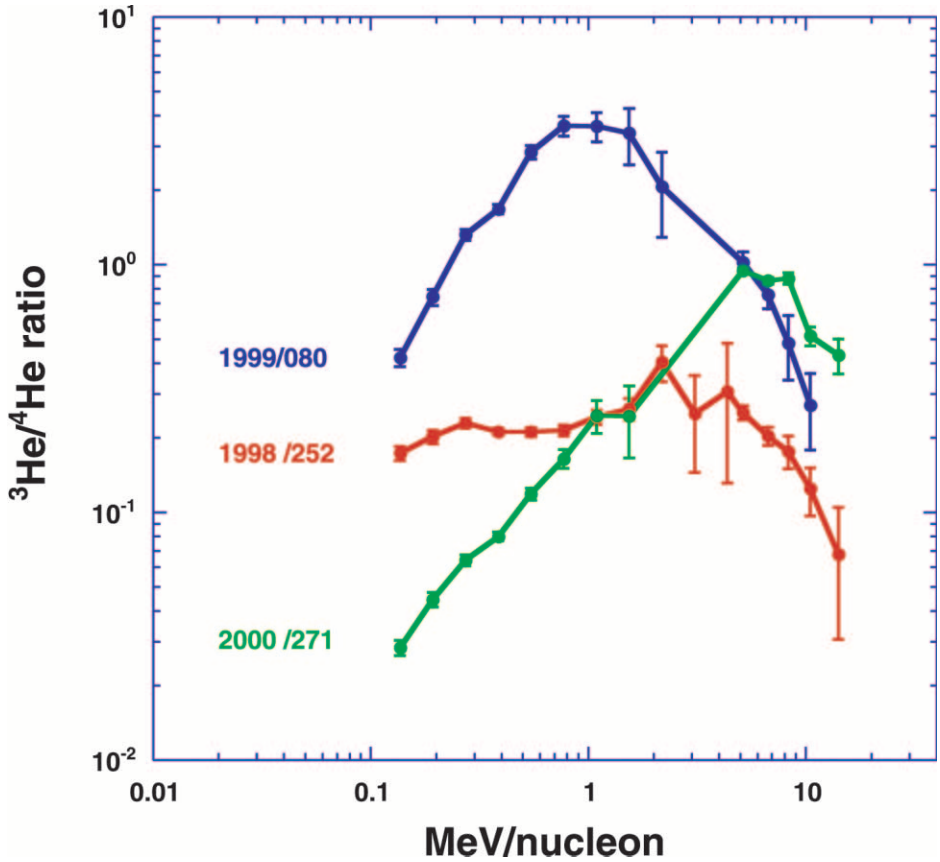

FIG. 8.—Energy dependence of the ^{3}He : ^{4}He ratio for the events shown in Figs. 4, 6, and 7

wind or large SEP events. The heavy-ion abundances are independent of the event class spectral features.

2.6. *Summary of Observations*

Our main observational results for the 14 events in this study may be summarized as follows (points 1–3 are summarized also in Table 3):

1. A total of 12 of the 14 events showed energy spectra of ^{3}He, ^{4}He, O, and Fe that are power laws or double power laws in energy per nucleon (≡class 1 events). Where there are double power laws, the energy spectrum becomes harder below 1 MeV nucleon^{-1}. At lower energies the spectral indices γ were notably harder, with $\Delta\gamma = 1.28 \pm 0.24$.

For these 12 class 1 events, the following applies:

a) Above ~1 MeV nucleon^{-1} the spectra were roughly similar, and above 1 MeV nucleon^{-1} the ^{3}He and ^{4}He spectra showed no systematic differences, with $\Delta\gamma = -0.15 \pm 0.51$, although there was considerable scatter; and

b) Below ~1 MeV nucleon^{-1}

i) eight events had ^{3}He spectral indices γ distinctly harder than other species; in many cases the ^{3}He spectral index γ was close to 1 and independent of the ^{4}He spectral index; the ^{3}He : ^{4}He ratio peaks in these events at energies from ~1 to a few MeV nucleon^{-1}, falling off at lower and higher energies; and

ii) the remaining four events had ^{3}He spectral indices close to that for other species; these events had significantly lower ^{3}He : ^{4}He ratios than the eight events with harder low-energy ^{3}He spectra.

2. Two of the 14 events had curved ^{3}He and Fe spectra that flattened notably at low energies (≡class 2 events), while the ^{4}He spectrum was a power law or double power law. The ^{3}He : ^{4}He ratio peaks in these events near 1 MeV nucleon^{-1}, falling off at lower and higher energies.

3. For both class 1 and class 2 events, ^{4}He and the heavy-ion spectra could be reasonably fitted by separate power laws in the ranges 0.1–1.0 and 1.0–10.0 MeV nucleon^{-1}.

4. At 375 keV nucleon^{-1} heavy-ion abundances were enhanced relative to gradual SEP events by a factor of ~2 for Ne–Si and by a factor of ~10 for Fe (normalized to O). There was no significant difference in heavy-ion enhancements between class 1 and class 2 events. The enhancements were similar to those seen in prior surveys at much higher energy and were reasonably ordered by mass or atomic number. The enhancements relative to gradual SEP events were not ordered by the FIP of the elements.

5. Time-intensity profiles for most of the events were "impulsive," indicating nearly scatter-free propagation, although at least one had a time-intensity profile that was similar to that for a large, CME-related event.

3. DISCUSSION

3.1. *Comparison with Previous Measurements*

Because ^{3}He-rich SEP events generally have low intensities, spectral measurements have been reported for only a

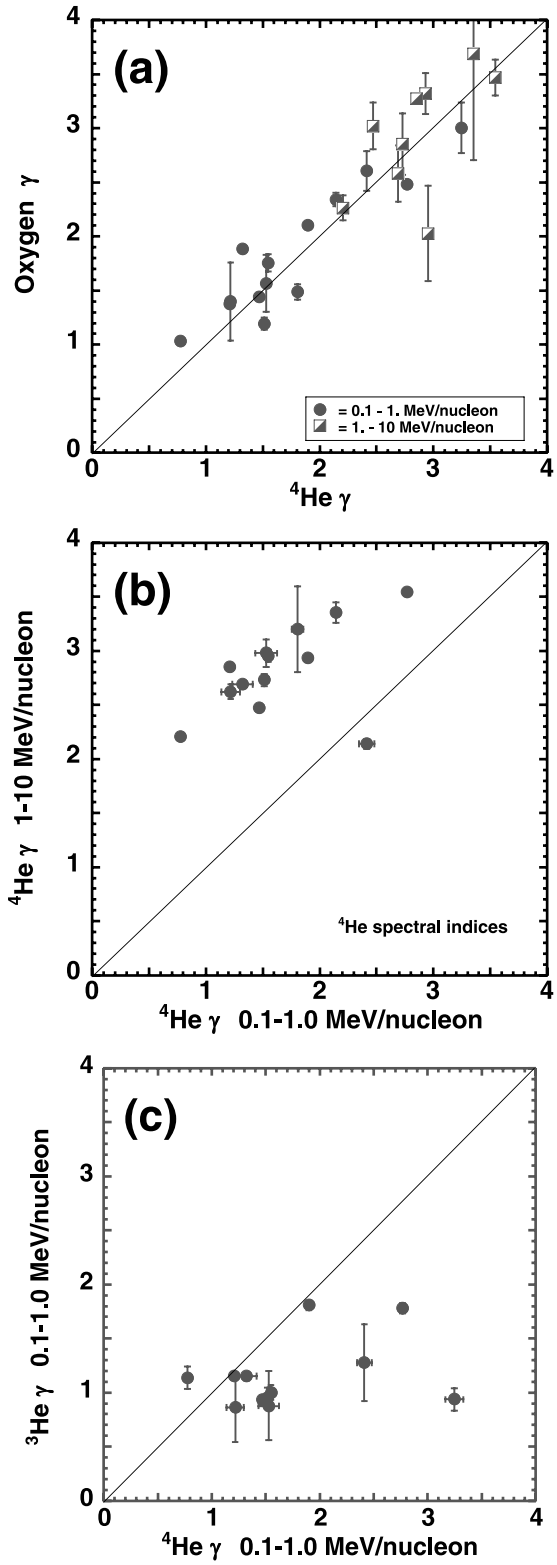

FIG. 9.—(*a*) Spectral index of oxygen vs. ^{4}He for 0.1–1.0 MeV nucleon^{-1} (*filled circles*) and 1–10 MeV nucleon^{-1} (*half-filled squares*). (*b*) Spectral index of 1–10 MeV nucleon^{-1} vs. 0.1–1.0 MeV nucleon^{-1} ^{4}He. (*c*) Spectral index of ^{3}He vs. ^{4}He for 0.1–1.0 MeV nucleon^{-1}.

small fraction of the observed events. The literature has contained occasional reports of ^{3}He-rich events that were also large SEP events, and indeed many of the reported spectral forms have been from such events because their intensities were high enough to allow a spectral measurement. A listing of large SEP events reported in the literature as also rich in ^{3}He is given in Table 4. The studies that reported spectral indices all had power laws for ^{3}He and ^{4}He that were similar. As an example, the three events in the study by Serlemitsos & Balasubrahmanyan (1975) all had ^{3}He and ^{4}He spectral indices that differed by less than 5%.

It can be seen from the table that the newer instruments on the *ACE* spacecraft have had the resolution to detect enrichments of ^{3}He that, although large, were still too small to have been observed by prior instruments. The study by Mason et al. (1999a) showed that the time-intensity profiles of ^{3}He and ^{4}He were similar in some large SEP events, thereby giving evidence that in these cases the ^{3}He acceleration and transport history was similar to that of the ^{4}He and other heavy ions. These authors concluded that remnant ^{3}He from small, impulsive solar particle events was being reaccelerated by CME-driven shocks in large SEP events whenever the shock moved through regions where impulsive flare suprathermals from prior events were still lingering. This mechanism for ^{3}He enhancements in large SEP events appears to be distinctly different than that operating in impulsive events, and so in comparing the present study with prior work, we set aside the cases of large ^{3}He-rich SEP events.

The two studies by Möbius et al. (1980, 1982) over the energy range 0.4–4 MeV nucleon^{-1} examined seven impulsive SEP events and found that the ^{3}He : ^{4}He ratio increased from 0.4 to ~2–6 MeV nucleon^{-1}; in some cases it was possible to extend the measurements to ~10 MeV nucleon^{-1}, and in these cases the ratio showed a drop. In all cases the He spectra continued to rise down to the 0.4 MeV nucleon^{-1} instrument threshold. The Möbius et al. study also examined O and Fe spectra. The overall trend in the spectra was that the ^{3}He was generally harder than ^{4}He (leading to the decrease at low energies) and the O spectrum was harder than the Fe spectrum. Why is it that the Möbius et al. study apparently did not find any events with ^{3}He spectra the same as other species as we have seen for some cases here? Probably this was due to the generally low ^{3}He : ^{4}He ratios in this type of event (see Table 1, events 2, 4, 11, and 12). As a result of the limited mass resolution of the instrument used by Möbius et al., these events probably would have been missed. Instrumental differences can also help explain why the Möbius et al. survey did not find any class 2 events: the key spectral features of these events lie at energies below the 400 keV nucleon^{-1} threshold of their instrument.

Another early survey reported that events with steep ^{3}He spectra tended to have larger ^{3}He : ^{4}He ratios (Reames & von Rosenvinge 1983). As an example of an event with steep spectra and high ^{3}He : ^{4}He ratio, the 1979 May 17 event had ^{3}He : ^{4}He ~ 12 with a power-law spectral index for ^{3}He of 2.7 ± 0.3 over the range 1.3–6 MeV nucleon^{-1} (Reames et al. 1985).

New instruments on the *SAMPEX* and *Wind* spacecraft extended the prior studies to both lower and higher energies. Reames et al. (1997a) examined five impulsive SEP events in early 1995 and found that the ^{3}He spectra were "rounded" toward low energies, although in all their cases the spectra continued to rise down to the instrument ^{3}He threshold of ~0.1 MeV nucleon^{-1}. Mazur et al. (1995) examined 11 impulsive SEP events and found that over the range 0.5–9.0 MeV nucleon^{-1} most of the Fe spectral shapes could be well fitted by power laws but in two cases the Ne–S and Fe spec-

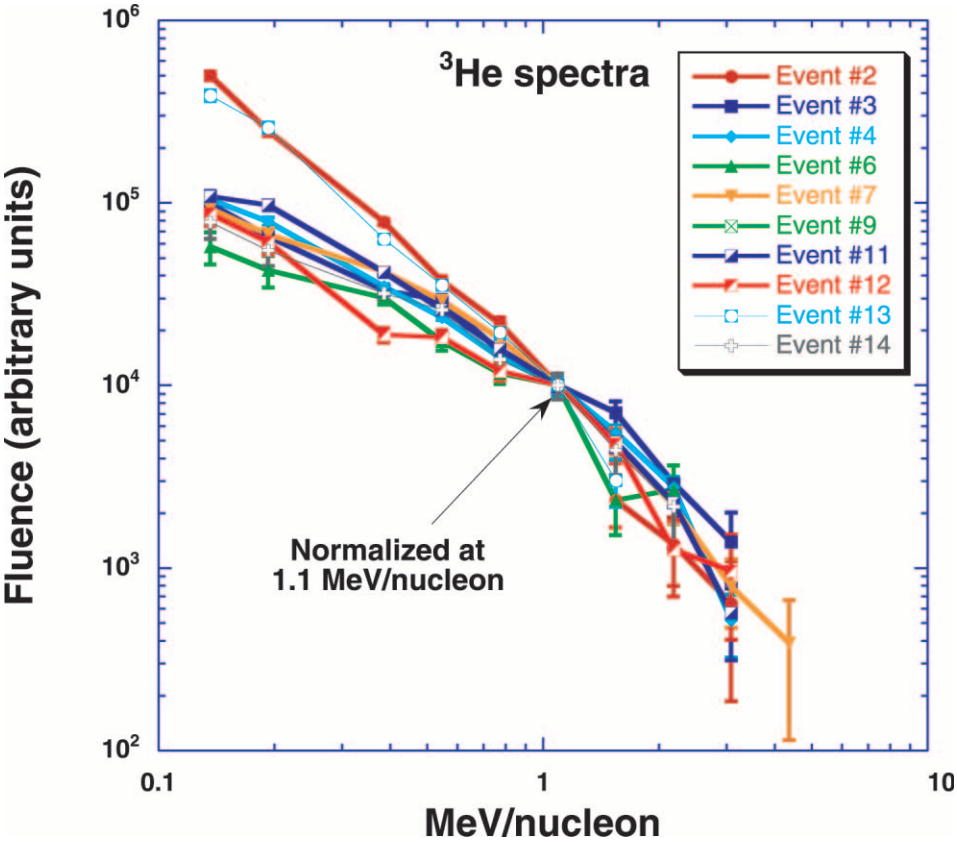

FIG. 10.—Spectra of ^{3}He of events 2–9 and 11–14 in Table 1, normalized to a fluence of 10^4 at 1.1 MeV nucleon^{-1}

tra rolled over toward low energies even though the O and He spectra in these events could be fitted by power laws. This behavior can be clearly seen in the two class 2 events in this study (e.g., Fig. 7*a*; see also Figs. 3 and 4 in Mason et al. 2000) where the ^{3}He and Fe spectra show a distinct curvature while ^{4}He and O can be reasonably fitted by power laws.

In our initial survey of ^{3}He-rich event spectra at energies below ~1 MeV nucleon^{-1} using *ACE* instruments (Mason et al. 2000), class 1 and class 2 events were iden-

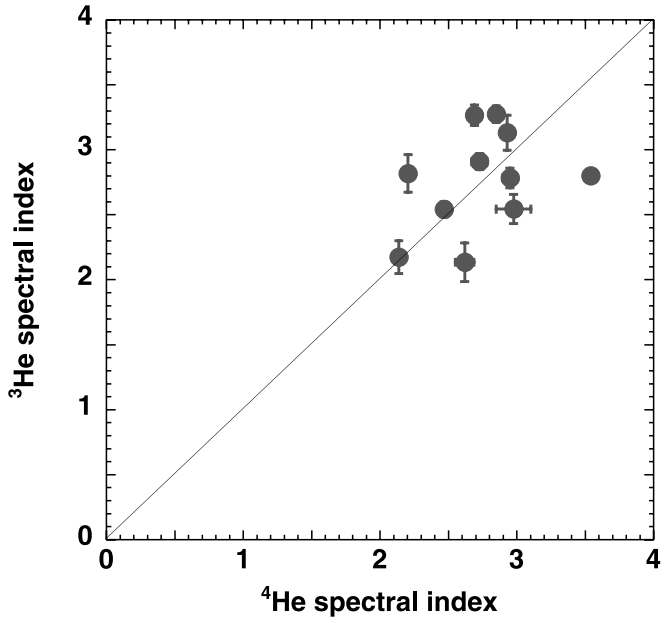

FIG. 11.—Spectral index of ^{3}He vs. ^{4}He for 1.0–10 MeV nucleon^{-1}

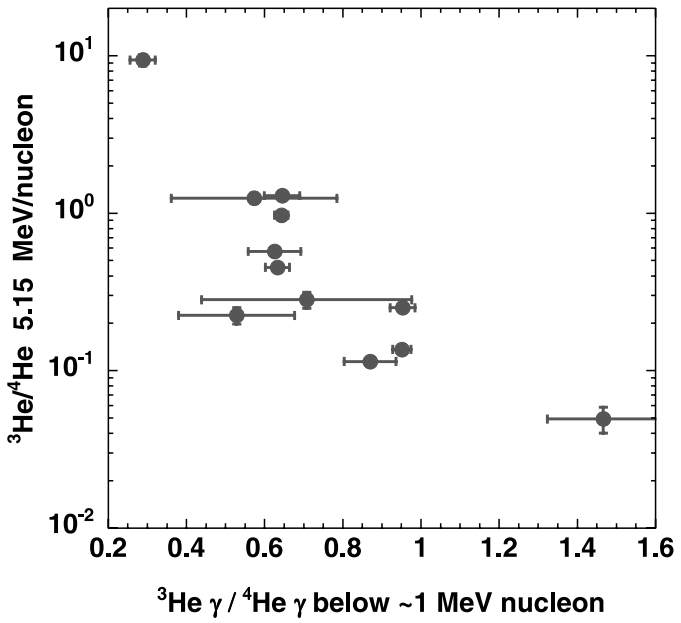

FIG. 12.—^{3}He : ^{4}He abundance ratio at 5.15 MeV nucleon^{-1} vs. ratio of low-energy spectral indices of ^{3}He and ^{4}He, showing that events with ^{3}He spectra harder than ^{4}He also tend to have high ^{3}He : ^{4}He ratios.

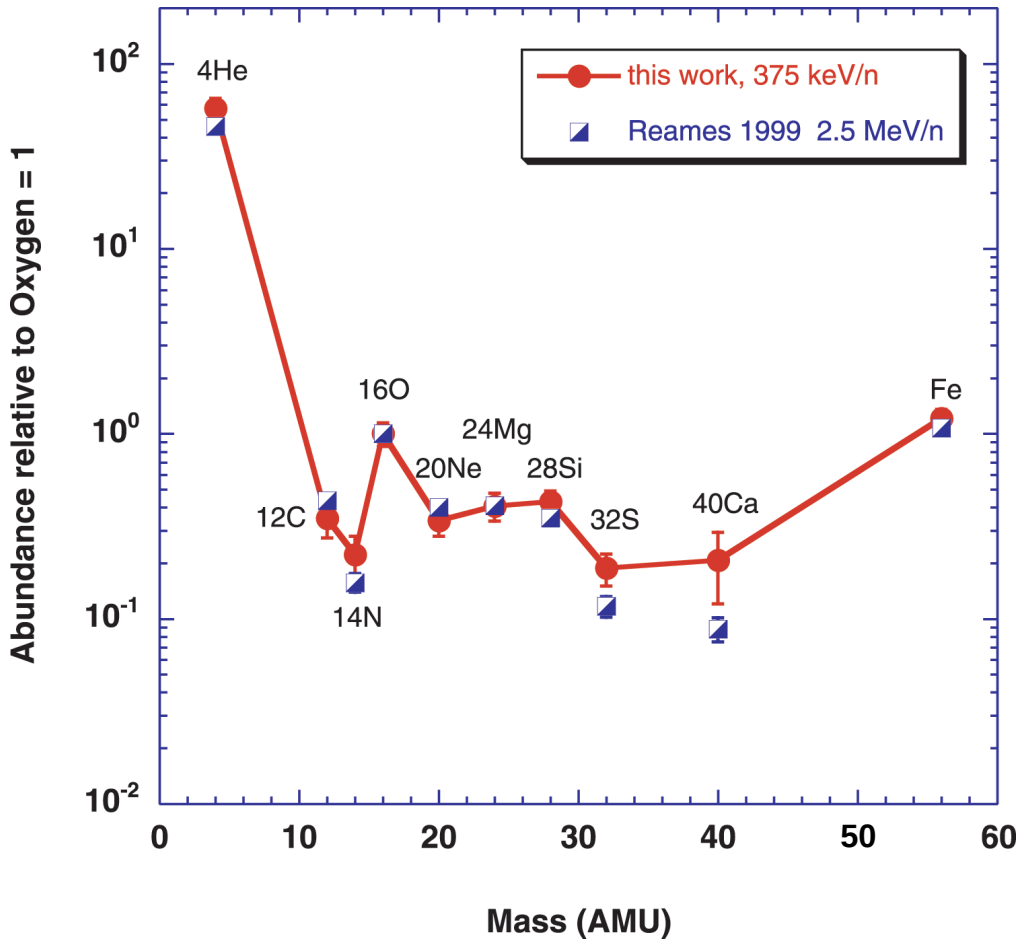

FIG. 13.—*Filled circles:* Average composition of ^{3}He-rich events at 375 keV nucleon^{-1} normalized to O ≡ 1; *half-filled squares:* average composition of impulsive ^{3}He-rich events at ~2.5 MeV nucleon^{-1} from Reames (1999).

tified. However, the frequency of occurrence of various types of events differs between this and the earlier study as can be seen from Table 5. The first column lists the spectral types, and the subsequent columns list the number of events of this type for the low-energy study (Mason et al. 2000), the present work, and the combined statistics for the two studies (note that three events, numbers 4, 8, and 12 in Table 1, were in both surveys). For the class 1 events, in the present study there were many more cases of low-energy ^{3}He spectra being harder than the ^{4}He spectra. While at first glance this would not appear to affect our event selection, we have seen that the events with harder low-energy ^{3}He spectra had larger ^{3}He : ^{4}He ratios at all energies and so indeed introduce a bias due to our requirement that SIS observe significant ^{3}He. Finally, the earlier study had many more class 2 events than the current one; this is undoubtedly due to our selection criteria: in the present study we required significant ^{3}He in the energy range of the SIS instrument, and for the curved class 2 spectra, the intensities fall off so steeply as to make it much less likely that there will be an observed increase at high energies, thus biasing against class 2 events. As a result of the biases introduced in the present survey by the requirement that SIS observe significant ^{3}He, the relative frequency of event occurrence is better represented by the earlier survey (the second column in Table 5).

3.2. *The Role of Interplanetary Propagation*

Interplanetary propagation must be considered in discussing our spectra because these forms can be modified in transit from the Sun to 1 AU. An extrapolation back to the Sun predicts enormous effects in terms of pitch-angle focusing and adiabatic deceleration (Ng & Wong 1979; Mason et al. 1989). Mazur et al. (1992) discussed this issue regarding somewhat higher energy data in large SEP events. For example, they estimated energy changes by adiabatic deceleration by about 50% at 1 MeV nucleon^{-1} and by less than 10% at 70 MeV nucleon^{-1}. In the present study the effects are potentially much larger at our lower energies, as a result of the increased transit time from the Sun.

However, the spectral forms that we observe indicate that interplanetary propagation is not dominating the shape, since we often see different spectral shapes in these events, especially in class 2 events. If propagation dominated, the spectral shapes would be expected to be more nearly similar. The question arises whether the class 1 events with similar spectral shapes are in fact dominated by propagation effects. While we cannot rule out this possibility, we note that the event with the cleanest, most nearly scatter-free propagation in the entire survey, namely, the 2000 May 1 event, had spectra of similar shapes for all elements. If any event in the survey would be expected to be free of propagation effects, that would be the one, and yet its spectral forms are not at all

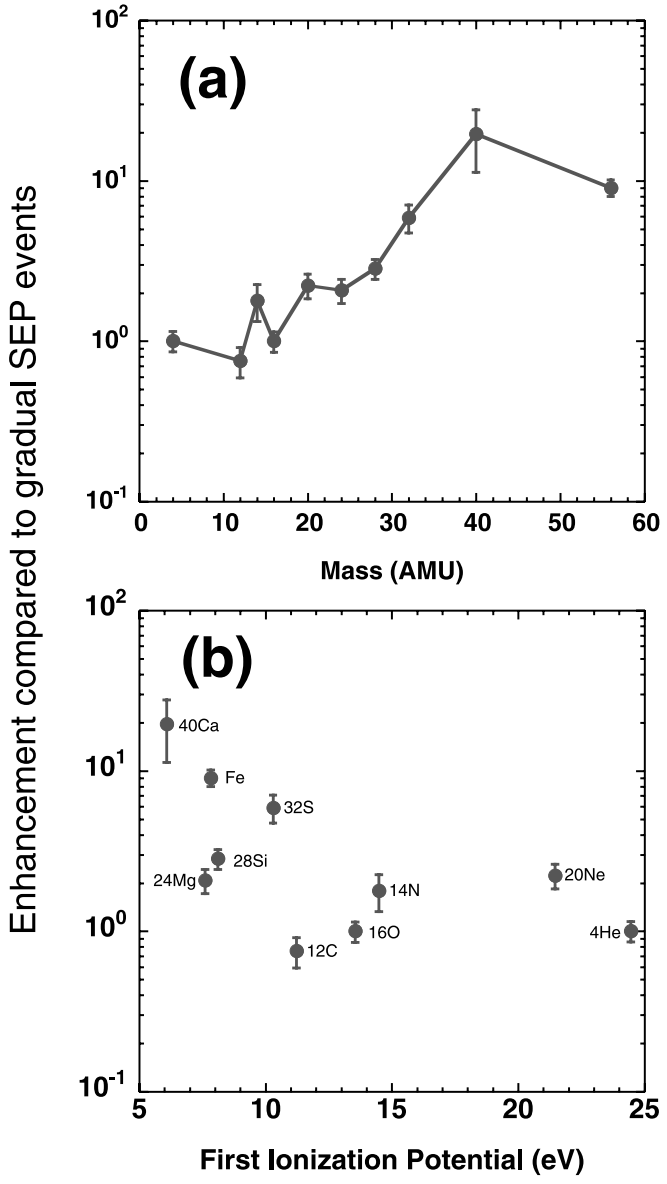

FIG. 14.—Enhancement of ^{3}He-rich events at 375 keV nucleon^{-1} (normalized to O $\equiv$ 1) relative to survey of large, gradual SEP events from Reames (1999) plotted vs. (*a*) mass and (*b*) FIP.

unusual. While a definitive resolution to these issues will require future observations in the inner solar system, we believe that the effects of propagation on these events are not large and that direct comparison with acceleration models, as done below, is meaningful.

3.3. *Class 1 Event Acceleration Mechanisms*

The rich variation in spectral properties of these events, in addition to their unique composition signatures, indicates that multiple mechanisms may be at work in the particle acceleration. While impulsive SEP events have previously been found to lack statistical association with coronal shocks and CMEs (Kahler et al. 1985), recent high-sensitivity measurements on *SOHO* have revealed at least one impulsive event (number 12 in Table 1) that was associated with a narrow CME (Kahler et al. 2001). However, the speed of this CME (960 km s^{-1}) may not have been sufficient to create a shock, and so the CME may be only a signature of coronal ejecta associated with an impulsive event and not the cause of the particle acceleration (Kahler et al. 2001).

The power-law spectra in the class 1 events show features of diffusive shock acceleration, including power-law shape, and changes of spectral slope. The first resonant heating model for ^{3}He-rich flares proposed selective heating by electrostatic ion cyclotron waves followed by an unspecified second-stage mechanism (Fisk 1978). This second-stage mechanism could in principle produce power-law spectra for all ions. In a recent modification of the Fisk theory, Zhang (1995) proposed a two-stage model for ^{3}He and heavy-ion enrichment due to current-driven electrostatic ion cyclotron instabilities that selectively preheat the ions and are then followed by acceleration to high energies by a Fermi process. Other recent models (Temerin & Roth 1992; Steinacker et al. 1997) have focused primarily on compositional signatures and would need to be reexamined to test predictions of spectral form.

Since shock acceleration models typically produce power-law spectra, they can clearly be constructed to model the class 1 spectra, provided there is an additional mechanism to explain the unique composition and charge state features of these events. However, it must be kept in mind that even in the case of the single impulsive particle event clearly associated with a CME, there was no detection of a shock, although the observations cannot rule out that possibility. The question remains regarding the two variants of class 1 events, namely, those with ^{3}He spectra similar to other species and those with ^{3}He spectra distinctly harder than other species in the range below $\sim$1 MeV nucleon^{-1}, leading to a decrease of the ^{3}He : ^{4}He ratio with decreasing energy. It may be significant that in a plasma of temperature $\sim 2 \times 10^6$ K the Coulomb losses reach their peak around $\sim$1 MeV nucleon^{-1} (Mullan 1980; Möbius et al. 1982), which is similar to the energy at which we observe a change in behavior of the spectra. Such decreases have been previously modeled using ionization energy loss as the mechanism, since the higher energy loss rate of ^{3}He compared to ^{4}He can lead to a decrease of this ratio at low energies (Kocharov & Kocharov 1984). These calculations can lead to a decrease in the ^{3}He : ^{4}He ratio below a few MeV nucleon^{-1}, with constant value at higher energies, which is typical of the spectra we observe. In addition, since the heavy-ion spectra all have a similar behavior below 1 MeV nucleon^{-1}, while in contrast the Coulomb energy loss rates for different species are quite different, it is not clear how Coulomb losses alone could explain the observed spectral feature (see also Korchak 1980). Models that involve both Coulomb losses and stochastic acceleration timescales have been explored by Möbius et al. (1982) and Ostryakov, Karatavykh, & Koval'tsov (2000). These models can produce quite complex spectral features and would require careful examination to see if they can provide reasonable fits to the observations presented here.

Another possibility mentioned in prior work (e.g., Reames 1993) and recently discussed by Mason et al. (2000) is that "all" the ambient ^{3}He is heated above some assumed injection threshold and this provides an upper limit on the ^{3}He : ^{4}He ratio. Clearly, if this were occurring, it could also affect the spectral form of ^{3}He differently from other species. If this is the case, it may be significant that the events with the different ^{3}He spectral slope at low energies almost invariably have larger ^{3}He : ^{4}He ratios at high energies than those

TABLE 3

SUMMARY OF ^{3}He-RICH EVENT PROPERTIES

PARAMETER	CLASS 1[a]		CLASS 2[b]
	Double Power Laws	Single Power Laws	
Example	See Fig. 4	See Fig. 6	See Fig. 7*a*
Number of cases in study	4	8	2
Spectral details	Spectra harden below $\sim$1 MeV nucleon^{-1}, with $\Delta\gamma = 1.28 \pm 0.24$	Single power law for all species except ^{3}He	
^{3}He spectra	Similar to other species	Slope harder than others below $\sim$1 MeV nucleon^{-1}, slope $\sim$1	^{3}He, Fe spectra curved
^{3}He : ^{4}He ratios	Lowest	. . .	Highest
^{3}He : ^{4}He energy dependence	Roughly constant with energy	Peaks from $\sim$1 to few MeV nucleon^{-1}	Peaks near $\sim$1 MeV nucleon^{-1}
Possible acceleration scenario	Further acceleration beyond single power-law case (?)	Next higher level acceleration (?)	Initial acceleration stage (?)

NOTE.—For both classes, ^{4}He spectra are single or double power laws; if there is a break, it occurs near 1 MeV nucleon^{-1}.

[a] ^{3}He power-law or double power-law spectra; above $\sim$1 MeV nucleon^{-1} all spectra are similar.

[b] ^{3}He, Fe spectra flatten notably at low energies.

TABLE 4
^{3}He-rich Large Solar Particle Events

Date	Energy Range (MeV nucleon^{-1})	^{3}He : ^{4}He Ratio (Typical)	Reference
1969 May 28–29 (three events).....	4–80	1.52 ± 0.1	1
		0.71 ± 0.06	
		0.35 ± 0.03	
1969 Oct 14	4–22.1	0.30 ± 0.06	2, 3
1970 Jul 30	10.5–22.1	0.54 ± 0.09	3
1980 Jun 21	6–60	$0.085^{+0.037}_{-0.026}$	4
1991 Mar 23–25 (three events)[a].....	50–100	0.043 ± 1.0	5
		0.050 ± 1.1	
		0.063 ± 0.6	
1997 Nov 2–6	0.5–2.0	$(1.9 \pm 0.5) \times 10^{-3}$	6
	8–14	8×10^{-3}	7
1997 Nov 6–10	0.5–2.0	$(2.1 \pm 0.8) \times 10^{-3}$	6
	8–14	7×10^{-3}	7
1998 May 2–4.....	0.5–2.0	0.013 ± 0.002	8
1998 May 6–8.....	0.5–2.0	$(3.5 \pm 0.7) \times 10^{-3}$	6
	8–14	0.04	7
1998 Nov 14–18	8–14	5×10^{-3}	7
1999 Jan 21–27.....	0.5–2.0	$(6.4 \pm 1.3) \times 10^{-3}$	8
1999 May 4–8.....		$(2.2 \pm 0.7) \times 10^{-3}$	
1999 Jun 2–3		0.055 ± 0.011	
1999 Jun 4–7		$(2.7 \pm 0.6) \times 10^{-3}$	

[a] 13 events reported in 1991 with ^{3}He : ^{4}He $> 0.5\%$; the three listed are those with the largest enhancements.

References.—(1) Serlemitsos & Balasubrahmanyan 1975. (2) Garrard et al. 1973. (3) Anglin 1975. (4) van Hollebeke, McDonald, & Meyer 1990. (5) Chen, Guzik, & Wefel 1995. (6) Mason et al. 1999a. (7) Cohen et al. 1999. (8) Mason et al. 1999b.

events that have ^{3}He spectra similar to the other ions. Thus, events where all the ^{3}He has been heated above the injection threshold will have higher ^{3}He : ^{4}He ratios at high energies and will also be relatively deficient in ^{3}He at low energies since the reservoir of low-energy particles was depleted by the heating. In other cases if not all the ^{3}He were preferentially heated, then ^{3}He and other ions all could have the same shape above the injection threshold, and one would then get similar spectral forms at all energies after the final acceleration. These cases with similar ^{3}He and other spectra at all energies would result in lower overall ^{3}He enhancements since the preheating did not affect all the ^{3}He.

3.4. *Class 2 Events: Stochastic Acceleration Mechanisms*

The class 2 events in this paper and the additional class 2 events discussed in Mason et al. (2000) have ^{3}He and Fe spectral shapes that are rounded at low energies. It is well known that this spectral form can arise from stochastic acceleration processes by Alfvén turbulence (e.g., review by Ramaty & Murphy 1987). Möbius et al. (1982) developed a stochastic model for ^{3}He-rich events. Mazur et al. (1992) modified the approach of Möbius et al. (1982) in a steady state model with energy and spatial diffusion coefficients of the same form as those of Möbius et al. (1982) but without explicit linkage to the magnetic field fluctuations that provide the scattering. Cast in this manner, Mazur et al. (1992) could include rigidity-dependent diffusion coefficients.

Following the notation of Mazur et al. (1992), the particle number density satisfies a diffusion equation with energy and spatial diffusion coefficients of

$$D(T, Q, A) = D_o \left(\frac{Q}{A}\right)^a T^b \tag{1}$$

and

$$\kappa(T, Q, A) = \kappa_o \left(\frac{Q}{A}\right)^{-a} T^{2-b} , \tag{2}$$

where T is energy per nucleon, Q is the charge state, A is the atomic mass, D_o is the energy diffusion coefficient, and κ_o is the spatial diffusion coefficient. Both D_o and κ_o are independent of time, particle energy, mass, and charge. The constants a and b are determined by fits to the spectra, and here we will use these forms to explore possible charge-to-mass dependence in the model. Mazur et al. (1992) show that the time-integrated differential flux resulting from this formulation is

$$j(T) = N_o T^{\alpha+1/2} K_\nu(\beta T^\gamma) , \tag{3}$$

where N_o is the spectral normalization, K_ν is the modified Bessel function of order ν, and the other parameters are defined in terms of the constants a and b by

$$\alpha = \frac{3 - 2b}{4} , \tag{4a}$$

$$\gamma = 2 - b , \tag{4b}$$

$$\nu = \frac{2b - 1}{4(2 - b)} , \tag{4c}$$

TABLE 5
Spectral Types in ^{3}He-rich Solar Particle Events

Spectral Signature	Number of Cases: Survey[a] below Few MeV nucleon^{-1}	This Work	Combined[b]
Class 1—power-law spectra:			
^{3}He spectral index similar to ^{4}He	5	4	6
^{3}He spectral index harder than ^{4}He below $\sim$1 MeV nucleon^{-1}	2	8	10
Class 2—curved ^{3}He spectra.....	5	2	7
Total in survey.....	12	14	23

[a] Mason et al. 2000.
[b] Three events listed in the second and third columns are in common, hence the combined number is not equal to the sum of the two columns.

and

$$\beta = \frac{1}{2-b}\frac{1}{L}\left(\frac{A}{Q}\right)^a \sqrt{\frac{\kappa_o}{D_o}}. \quad (4d)$$

In equation (4d) L is the length scale of the acceleration region. The spectral form in equation (3) can be compared directly to our event-averaged spectra. In fitting the energy spectra we determine values of β (eq. [4d]) and b (eqs. [1] and [2]): β gives the A/Q dependence of the diffusion coefficients, while b determines the energy dependence of the diffusion coefficients.

In a study of large SEP events Mazur et al. (1992) found that b showed little dependence on species and in nine events varied over the range 1.56 ± 0.02 to 1.86 ± 02. The parameter β varied from one event to the next and also varied among species in individual events, as a result of the generally faster falloff of heavier elements with increasing energy. The values of β for Fe ranged from 5.24 ± 0.11 to 16.08 ± 0.18 and were always greater than those for H and He, by amounts up to a factor of $\sim$2. While the acceleration in these large events is believed to be due to different processes than in impulsive SEP events, these values of b and β nonetheless give an idea of typical fitting results for large SEP events.

Figure 15 shows a sample fit to the 1999 August 7 class 2 event (number 8). The fits are quite reasonable for the lower energy portion of the spectra, but in both cases the observed spectra show a high-energy tail that is not fitted by the model. The best-fit parameters are $b = 1.01 \pm 0.04$, $\beta = 1.67 \pm 0.08$ for ^{3}He and $b = 1.16 \pm 0.07$, $\beta = 4.91 \pm 0.54$ for Fe. Compared to large particle event fits, the small values of b in both cases correspond to relatively faster diffusion out of the acceleration site along with slower energy diffusion, both combining to result in spectral falloffs at relatively low energies. The two β parameters can be used to derive the dependence of the diffusion coefficients on A/Q. Assuming that the ^{3}He are fully stripped and that the Fe charge state is +20, the derived value for $a = 2.0$, so the energy diffusion, is proportional to $(Q/A)^{2.0}$. This leads to the markedly smaller energization of Fe compared to ^{3}He. Although the fits to the low-energy portions of the ^{3}He spectrum are reasonable, this model does not explain the high-energy tail in either case. Neither does this model explain the power-law shape for ^{4}He: if we were to estimate the ^{4}He spectral shape based on the ^{3}He and Fe, we would find a curved spectrum whose shape lay between ^{3}He and Fe; however, this is not what is observed.

3.5. *Class 2 Events: Cascading MHD Turbulence Acceleration Mechanism*

The problem of fitting the remaining heavy-ion species may require a separate mechanism, which is also suggested by the differences in spectral shape. Miller (1998) has proposed such a mechanism that involves cascading MHD turbulence. The cascading turbulence model has been shown previously (e.g., Miller & Roberts 1995; Miller, LaRosa, & Moore 1996; Miller 2000) to account for all the bulk features (such as acceleration timescales, fluxes, total number of energetic particles, and maximum energy) of electron and proton acceleration in impulsive solar flares. While the

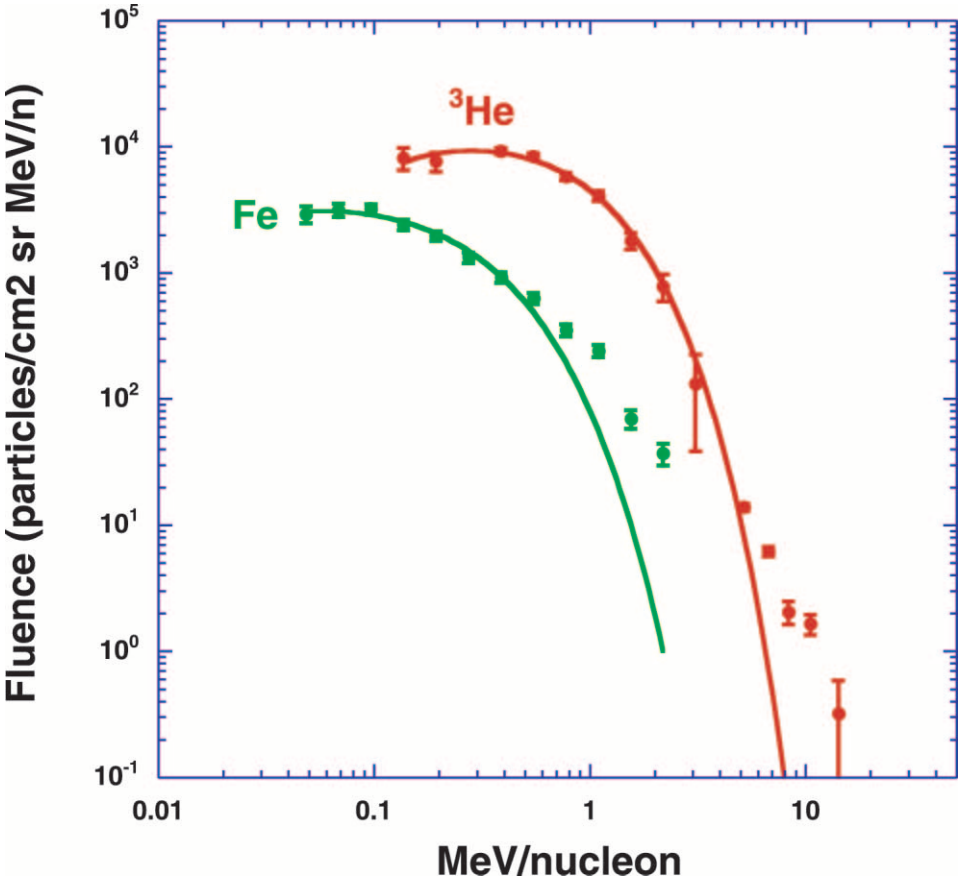

FIG. 15.—^{3}He (*red*) and Fe (*green*) spectra from event 8 compared with calculated spectra for a stochastic acceleration model

simulation of this acceleration process is rather involved, the essential idea of the model is quite simple and consists of just a few parts:

1. During the primary flare energy release phase, we assume that low-amplitude MHD Alfvén and fast-mode waves are excited at long wavelengths, say, comparable to the size of the region producing the event (although the results are actually insensitive to this initial wavelength). While an assumption, this appears reasonable in light of the likely highly turbulent nature of the flare.

2. These waves then cascade in a Kolmogorov-like fashion to smaller wavelengths (e.g., Verma et al. 1996), forming a power-law spectral density in wavenumber space through the inertial range.

3. When the mean wavenumber of the fast-mode waves has increased sufficiently, the transit-time acceleration rate (Miller 1997) for super-Alfvénic electrons can overcome Coulomb energy losses, and these electrons are accelerated out of the thermal distribution and to relativistic energies (Miller et al. 1996). As the Alfvén waves cascade to higher wavenumbers, they can cyclotron resonate with progressively lower energy protons. Eventually, they will resonate with protons in the tail of the thermal distribution, which will then be accelerated to relativistic energies as well (Miller & Roberts 1995). Hence, both ions and electrons are stochastically accelerated, albeit by different mechanisms and different waves.

4. When the protons become super-Alfvénic (above $\approx$1 MeV nucleon^{-1}), they too can suffer transit-time acceleration by the fast-mode waves and will receive an extra acceleration "kick."

We envisage this acceleration process as occurring in the coronal portion of the flare loop, which is modeled by an ionized homogeneous plasma extending a distance L along a constant magnetic field $\boldsymbol{B}$. An important aspect of stochastic acceleration in general is that it is not directed, as with DC electric fields. This allows cospatial return currents to form, which draw particles up from the denser and cooler chromosphere, ensure charge neutrality, and provide the replenishment for the acceleration region that is necessary to sustain the large fluxes observed in some flares. We model this acceleration process with a self-consistent quasi-linear simulation, in which stochastic particle acceleration, particle escape from the acceleration region, Coulomb collisions, wave cascading, wave damping by the particles, and acceleration region replenishment are all taken into account. We find that this model will account for all the major features of the energetic particles from even the largest impulsive solar flares. This is true for a broad range of plasma density and magnetic field values, provided that sufficient power is input into both Alfvén and fast-mode waves (>400 ergs cm^{-3} s^{-1}) and that the acceleration region is sufficiently small (up to several times 10^8 cm).

However, perhaps the strongest point in favor of this cascading turbulence model is its ability to account for the acceleration of heavier (with the exception of ^{3}He) ions as well. As was pointed out by Reames et al. (1994), at a temperature of around 3×10^6 K, there is a threefold separation of gyrofrequencies among the heavy ions. Specifically, the charge-to-mass Q/A ratio of Fe is around 0.23; that of Ne, Mg, and Si is about 0.4; and that of ^{4}He, C, N, and O is 0.5. Indeed, such a separation appears to be a necessary precondition for selective enhancements in the energetic particles, regardless of the actual acceleration mechanism. It also allows specifically the framework of the cascading turbulence model to naturally yield the observed enhancements. Qualitatively, in a multi-ion flare plasma, the Alfvén waves, which cascade from low to high frequencies, will encounter Fe first. Iron will be strongly accelerated but is not abundant enough to damp the waves. Thus, some wave energy will cascade to higher frequencies where it encounters Ne, Mg, and Si next. In the same way, these ions suffer strong (but not as strong as that for Fe) acceleration, but the wave dissipation is not complete. Some wave energy then cascades to reach ^{4}He, C, N, and O, which are then also stochastically accelerated out of the background plasma but resonate with waves that have been somewhat dissipated as a result of the ions at lower Q/A. Thus, Fe will resonate with the most powerful waves; Ne, Mg, and Si will resonate with waves having less power; and the other heavies will resonate with even less powerful waves. Hence, Fe should be enhanced more than the Ne group relative to the He group. Since ^{4}He, C, N, and O all have the same cyclotron frequency and behave similarly, they should not be enhanced relative to each other.

The quasi-linear simulation has been extended to include the heavy-ion species as well, and the numerical results support the above scenario. As an example, we take $\boldsymbol{B} = 500$ G, the Alfvén speed $v_A = 0.036c$, the temperature of the plasma to be initially 3×10^6 K, and the H density to be 10^{10} cm^{-3}, which remains constant as a result of the return current. The waves are injected at a wavelength of 10^7 cm; however, as discussed in Miller & Roberts (1995), the nature of the particle acceleration is independent of this specific wavelength. We do not regard these parameters as free, since changes in their values can be compensated for by changes in the total wave energy density injection rate P and the length scale of the acceleration region L such that the results do not change appreciably. Hence, *this simulation has only two free parameters, P and L*. For $P \approx 40$ ergs cm^{-3} s^{-1} and $L \approx 10^8$ cm, the enhancements in the Fe/O ratio in the energetic particles (>1 MeV nucleon^{-1}) are about 10–13, while the Ne/O, Mg/O, and Si/O ratios are enhanced by about 3–6; ^{4}He, C, N, and O are not enhanced relative to each other. These integrated enhancements are fairly typical of those observed for impulsive or ^{3}He-rich flares.

We do not take into account charge exchange reactions or any other process that affects the ion charge states in the simulation, and so the Fe charge of +13 (which corresponds to an initial plasma temperature of 3 MK) remains, fixed, as do the charge states of the other ions. In order to reconcile this charge state with that typically observed for impulsive events (around +20), there must be additional stripping that occurs during or after the ion acceleration. Specifically, it must occur after the time it takes the waves to cascade through Fe, Ne, Mg, and Si and accelerate these heaviest ions out of the thermal distribution and to moderately suprathermal energies. This, in turn, happens in less than a second after the waves are produced at low wavenumbers. At the end of this time, the enhancements are more or less "frozen in," and a change in the charge states should not greatly affect the abundances in the energetic particles. Hence, a stripping timescale greater than about a second should not qualitatively affect our results. We do not address the issue of what causes this additional stripping, but one possibility is given in Miller & Viñas (1993), where it was pointed out that an electron beam (which is ultimately

responsible for the ^{3}He enhancements) would also lead to further ionization of Fe to a charge state of about +20 on a timescale of a few seconds.

In Figure 16 we show a comparison between the theoretical fluxes of He, O, Ne, and Fe and those observed with ULEIS and SIS for the 1999 August 7 class 2 flare. The model distributions were obtained with $P = 191$ ergs cm^{-3} s^{-1} and $L = 10^8$ cm. The spectral forms of the theoretical fluxes, along with their relative normalizations, are determined by the simulation; the absolute normalization is arbitrary (since it is proportional to the duration of the acceleration process) and is varied so as to obtain the best fit to the observed spectra. The results for all four species are very encouraging (considering that this is just a two-parameter fit), but particularly so for Fe, Ne, and O. The low-energy rollover of Fe is reproduced well. This rollover results from the wholesale convection of the background Fe ions to higher energies when the waves cascade through the distribution. In fact, this rollover is apparent in all the spectra but moves to slightly lower energies as Q/A for the ions increases. This, in turn, results from the ions resonating with lower amplitude waves and not being able to be accelerated to as high an energy before escaping from the region.

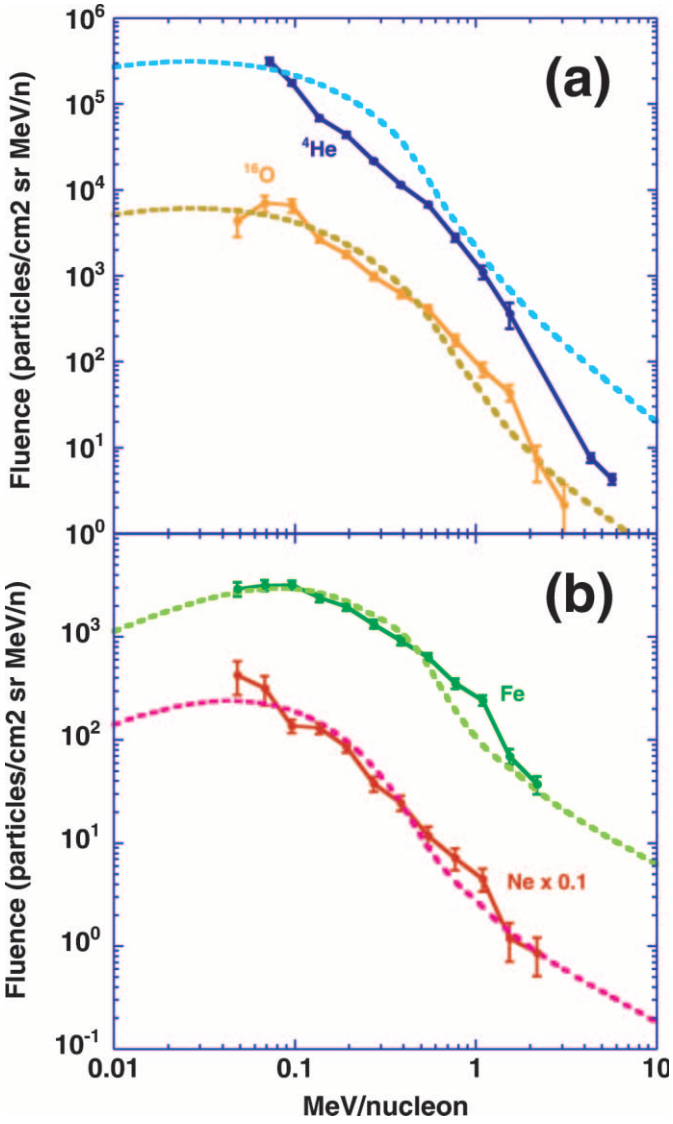

FIG. 16.—Comparison of spectra from event 8 with spectra calculated using a model of cascading MHD turbulence. (*a*) ^{4}He and O; (*b*) Ne (multiplied by 0.1) and Fe.

The fit is not as good at high energies, where the model spectra are much harder than those observed. This spectral hardness is the result of the ions resonating with the fast-mode waves above a few MeV nucleon^{-1}, and thus receiving basically a "double dose" of acceleration in this regime. This is in contrast to the stochastic acceleration spectra in Figure 15, which fall well below the observations at higher energies. Further refinement of the cascading MHD turbulence model may improve the high-energy fit, but even as it stands it gives the prospect of reconciling the curved low-energy spectra with the higher energy power law seen in several events.

4. SUMMARY AND CONCLUSIONS

Our survey of ^{3}He-rich solar particle event spectra using instruments with higher sensitivity and resolution than previous work has established two classes of events. Class 1 exhibits power laws that often steepen above ~1 MeV nucleon^{-1}; in some cases the major species ^{3}He, ^{4}He, O, and Fe have similar spectral slopes, while in others the ^{3}He spectral slope is distinctly harder than the others in the range below ~1 MeV nucleon^{-1}. Class 2 events show curved ^{3}He and Fe spectra, while ^{4}He has power-law spectra; the largest ^{3}He : ^{4}He ratios are found in class 2 events. Models of selective preheating of ^{3}He followed by a second-stage acceleration may be sufficient to fit the class 1 spectra, although the additional hardening of the ^{3}He requires explanation in this case. The class 2 event ^{3}He and Fe low-energy spectra, which roll over toward low energy, can be fitted by a stochastic acceleration model, but this leaves open the mechanism that explains the ^{4}He and O spectra in these same events, which are more like power laws. Models based on cascading MHD turbulence give promising fits to the class 2 heavy-ion spectra; these models require a further mechanism to provide the large enhancements of ^{3}He.

It may be that the class 2 events give us our closest look into the basic ^{3}He enrichment mechanism and that the class 1 events represent further stages of acceleration that modify the spectra. This is suggested by the pattern wherein the largest ^{3}He enrichments are in the class 2 events, followed by the class 1 with harder ^{3}He spectra at low energy, followed at the end by the events with similar power laws for all species.

In that sense, there may be a further step in this series, namely, the large, shock-associated SEP events that also show significant ^{3}He enrichments that are smaller than those in the present survey. The large ^{3}He-rich SEP events in effect represent the final processing of ^{3}He-enriched material by interplanetary shocks, while the class 1 and class 2 events studied here are probing processes in coronal loops or elsewhere close to the flare site itself.

We thank the many individuals at the University of Maryland, Johns Hopkins Applied Physics Laboratory, California Institute of Technology, Jet Propulsion Laboratory, and Goddard Space Flight Center responsible for the construction of the ULEIS and SIS instruments. This work was supported in part by NASA under grant PC 251429 at the University of Maryland and NAG 5-6912 at Caltech.

REFERENCES

Anglin, J. D. 1975, ApJ, 198, 733
Breneman, H. H., & Stone, E. C. 1985, ApJ, 299, L57
Chen, J., Guzik, T. G., & Wefel, J. P. 1995, ApJ, 442, 875
Cohen, C. M. S., Mewaldt, R. A., Leske, R. A., Cummings, A. C., Stone, E. C., Wiedenbeck, M. E., Christian, E. R., & von Rosenvinge, T. T. 1999, Geophys. Res. Lett., 26, 2697
Desai, M. I., Mason, G. M., Dwyer, J. R., Mazur, J. E., Smith, C. W., & Skoug, R. M. 2001, ApJ, 553, L89
Fisk, L. A. 1978, ApJ, 224, 1048
Garrard, T. L., Stone, E. C., & Vogt, R. E. 1973, in High Energy Phenomena on the Sun, ed. R. Ramaty et al. (NASA SP-342), 341
Kahler, S., Reames, D. V., Sheeley, N. R., Jr., Howard, R. A., Kooman, M. J., & Michels, D. J. 1985, ApJ, 290, 742
Kahler, S. W., Reames, D. V., & Sheeley, N. R., Jr. 2001, ApJ, 562, 558
Kocharov, L. G., & Kocharov, G. E. 1984, Space Sci. Rev., 38, 89
Korchak, A. A. 1980, Sol. Phys., 66, 149
Larson, D. E., et al. 1997, Adv. Space Res., 20, 655
Luhn, A., et al. 1985, Proc. 19th Int. Cosmic-Ray Conf., 4, 241
Mason, G. M., Dwyer, J. R., & Mazur, J. E. 2000, ApJ, 545, L157
Mason, G. M., et al. 1998, Space Sci. Rev., 86, 409
———. 1999a, Geophys. Res. Lett., 26, 141
Mason, G. M., Mazur, J. E., & Dwyer, J. R. 1999b, ApJ, 525, L133
Mason, G. M., Mazur, J. E., Dwyer, J. R., Reames, D. V., & von Rosenvinge, T. T. 1997, ApJ, 486, L149
Mason, G. M., Ng, C. K., Klecker, B., & Green, G. 1989, ApJ, 339, 529
Mason, G. M., Reames, D. V., Klecker, B., Hovestadt, D., & von Rosenvinge, T. T. 1986, ApJ, 303, 849
Mazur, J. E., Mason, G. M., Dwyer, J. R., Giacalone, J., Jokipii, J. R., & Stone, E. C. 2000, ApJ, 532, L79
Mazur, J. E., Mason, G. M., & Klecker, B. 1995, ApJ, 448, L53
Mazur, J. E., Mason, G. M., Klecker, B., & McGuire, R. E. 1992, ApJ, 401, 398
Miller, J. A. 1997, ApJ, 491, 939
———. 1998, Space Sci. Rev., 86, 79
———. 2002, in ASP Conf. Ser. 206, High Energy Solar Physics: Anticipating HESSI, ed. R. Ramaty et al. (San Francisco: ASP), 145
Miller, J. A., LaRosa, T. N., & Moore, R. L. 1996, ApJ, 461, 445
Miller, J. A., & Roberts, D. A. 1995, ApJ, 452, 912
Miller, J. A., & Viñas, A. F. 1993, ApJ, 412, 386
Miller, J. A., Viñas, A. F., & Reames, D. V. 1993, Proc. 23d Int. Cosmic-Ray Conf., 3, 13
Möbius, E., et al. 1999, Proc. 26th Int. Cosmic-Ray Conf., 6, 87
———. 2000, AIP Conf. Proc. 528, Acceleration and Transport of Energetic Particles Observed in the Heliosphere, ed. R. A. Mewaldt et al. (New York: AIP), 131
Möbius, E., Hovestadt, D., Klecker, B., & Gloeckler, G. 1980, ApJ, 238, 768
Möbius, E., Scholer, M., Hovestadt, D., Klecker, B., & Gloeckler, G. 1982, ApJ, 259, 397
Mullan, D. J. 1980, ApJ, 237, 244
Ng, C. K., & Wong, K.-Y. 1979, Proc. 16th Int. Cosmic-Ray Conf., 5, 252
Ostryakov, V. M., Karatavykh, Y. Y., & Koval'tsov, G. A. 2000, Astron. Lett., 26, 122
Ramaty, R., & Murphy, R. J. 1987, Space Sci. Rev., 45, 213
Reames, D. V. 1993, Adv. Space Res., 13, 331
———. 1995, Adv. Space Res., 15(7), 41
———. 1999, Space Sci. Rev., 90, 413
Reames, D. V., Barbier, L. M., von Rosenvinge, T. T., Mason, G. M., Mazur, J. E., & Dwyer, J. R. 1997a, ApJ, 483, 515
Reames, D. V., Meyer, J. P., & von Rosenvinge, T. T. 1994, ApJS, 90, 649
Reames, D. V., Ng, C. K., Mason, G. M., Dwyer, J. R., Mazur, J. E., & von Rosenvinge, T. T. 1997b, Geophys. Res. Lett., 24, 2917
Reames, D. V., & von Rosenvinge, T. T. 1983, Proc. 18th Int. Cosmic-Ray Conf., 4, 48
Reames, D. V., von Rosenvinge, T. T., & Lin, R. P. 1985, ApJ, 292, 716
Richardson, I. G., Dvornikov, V. M., Sdobnov, V. E., & Cane, H. V. 2000, J. Geophys. Res., 105, 12579
Serlemitsos, A. T., & Balasubrahmanyan, V. K. 1975, ApJ, 198, 195
Steinacker, J., Meyer, J.-P., Steinacker, A., & Reames, D. V. 1997, ApJ, 476, 403
Stone, E. C., et al. 1998a, Space Sci. Rev., 86, 357
Stone, E. C., Frandsen, A. M., Mewaldt, R. A., Christian, E. R., Margolies, D., Ormes, J. F., & Snow, F. 1998b, Space Sci. Rev., 86, 1
Temerin, M., & Roth, I. 1992, ApJ, 391, L105
van Hollebeke, M. A. I., McDonald, F. B., & Meyer, J. P. 1990, ApJS, 73, 285
Varvoglis, H., & Papadopoulos, K. 1983, ApJ, 270, L95
Verma, M. K., Roberts, D. A., Goldstein, M. L., Ghosh, S., & Stribling, W. T. 1996, J. Geophys. Res., 101, 21619
von Steiger, R., & Geiss, J. 1989, A&A, 225, 222
von Steiger, R., Geiss, J., & Gloeckler, G. 1997, in Cosmic Winds and the Heliosphere, ed. J. R. Jokipii et al. (Tucson: Univ. Arizona Press), 581
Wiedenbeck, M. E., et al. 2000, in AIP Conf. Proc. 528, Acceleration and Transport of Energetic Particles Observed in the Heliosphere, ed. R. A. Mewaldt et al. (New York: AIP), 131
Zhang, T. X. 1995, ApJ, 449, 916
Zwickl, R., Roelof, E. C., Gold, R. E., Krimigis, S. M., & Armstrong, T. P. 1978, ApJ, 225, 281